Microbiome Inhibition of IRAK-4 by Trimethylamine Mediates Metabolic and Immune Benefits in High-Fat-Diet-induced Insulin Resistance

Julien Chilloux[1,8], Francois Brial[2,8], Amandine Everard[3,8], David Smyth[4,8], Liyong Zhang[4], Hubert Plovier[3], Antonis Myridakis[1], Lesley Hoyles[1], Julian E. Fuchs[5], Christine Blancher[6], Selin Gencer[1], Laura Martinez-Gili[1], Jane F. Fearnside[6], Richard H. Barton[1], Ana Luisa Neves[1], Alice R. Rothwell[6], Christelle Gérard[2], Sophie Calderari[2], Claire L. Boulangé[1], Saroor Patel[1], James Scott[7], Robert C. Glen[1,5], Nigel J. Gooderham[1], Jeremy K. Nicholson[1], Dominique Gauguier[1,2,6,9], Peter P. Liu[4,9], Patrice D. Cani[1,3,9], Marc-Emmanuel Dumas[1,9¶]

[1] Integrative Systems Medicine and Digestive Disease, Department of Surgery and Cancer, Imperial College London, Exhibition Road, South Kensington, London SW7 2AZ, United Kingdom, [2] Sorbonne Universities, University Pierre & Marie Curie, University Paris Descartes, Sorbonne Paris Cité, INSERM UMR_S1138, Cordeliers Research Centre, 15 rue de l'Ecole de Médecine, 75006 Paris, France, [3] Université catholique de Louvain, Louvain Drug Research Institute, WELBIO (Walloon Excellence in Life sciences and BIOtechnology), Metabolism and Nutrition Research Group, 1200 Brussels, Belgium, [3] University of Ottawa Heart Institute, Ottawa ON K1Y 4W7, Canada, [5] Centre for Molecular Informatics, Department of Chemistry, University of Cambridge, Lensfield Road, Cambridge CB2 1EW, UK, [6] Wellcome Trust Centre for Human Genetics, Roosevelt Drive, University of Oxford, Oxford OX3 7BN, UK, [7] Imperial College London, National Heart and Lung Institute, Hammersmith Hospital, London, UK.

[8] these authors contributed equally and should be considered as co-first authors

[9] these authors contributed equally and should be considered as co-senior authors

¶ correspondence should be addressed to M.-E.D.: m.dumas@imperial.ac.uk

Referenced abstract

The interaction between high-fat diet (HFD) feeding and the gut microbiome has a strong impact on the onset of insulin resistance (IR)[1-3]. In particular, bacterial lipopolysaccharides (LPS) and dietary fats trigger low-grade inflammation[4] through activation of *Toll*-like receptor 4 (TLR4), a process called metabolic endotoxemia[5]. However, little is known about how the microbiome can mitigate this process. Here, we investigate longitudinal physiological and metabotypical responses of C57BL/6 mice to HFD feeding. A series of *in vivo* experiments with choline supplementation, then blocking trimethylamine (TMA) production and administering TMA, demonstrate that this microbiome-associated metabolite decouples inflammation and IR from obesity in HFD. Through *in vitro* kinome screens and *in silico* molecular dynamics studies, we reveal TMA specifically inhibits Interleukin-1 Receptor-associated Kinase 4 (IRAK-4), a central kinase integrating signals from various TLRs and cytokine receptors. Consistent with this, genetic ablation and chemical inhibition of IRAK-4 result in similar metabolic and immune improvements in HFD. In summary, TMA appears as a key microbial effector inhibiting IRAK-4 and mediating metabolic and immune effects with benefits upon HFD. Thereby we highlight the critical contribution of the microbial signalling metabolome in homeostatic regulation of host disease and the emerging role of the kinome[6] in microbial–mammalian chemical crosstalk.

Main Text

IR is key to a cluster of conditions such as impaired glucose tolerance (IGT), obesity, hyperlipidemia, hypertension and non-alcoholic fatty liver disease (NAFLD), increasing the risk of developing type 2 diabetes and cardiovascular diseases[7]. One of the hallmarks of these disorders is the early development of a systemic low-grade inflammation[4]. Increasing evidence supports that complex communication occurs between the gut microbiota and the innate immune system[8], with consequences on metabolic homeostasis[9]. Whilst some of the functional signalling molecules mediating microbial–mammalian chemical crosstalk have been characterized, a limited number of metabolite classes and their targets have been identified (G protein-coupled[10] and nuclear[11] receptors). It is, however, hypothesized that microbial metabolites potentially affect other pharmacological target classes such as kinases[6]. In previous studies, we and others have identified a family of

60 microbiome-associated metabolites, methylamines, associated with IR, NAFLD[12] and
61 atherosclerosis[13], but their mechanisms of action on mammalian hosts remain unclear.
62 TMA is one of the most abundant microbial metabolites produced by the gut microbiota.
63 We first reported that TMA may be associated with IR[12]. TMA results from microbial
64 metabolism of dietary choline, carnitine and TMAO[14-18] before being absorbed and *N*-
65 oxidized into TMAO by hepatic flavin-containing mono-oxygenase 3 (FMO3)[19]. After initial
66 reports associating TMAO with adverse cardiovascular outcomes[13,16], it has since emerged
67 that Fmo3 inactivation was beneficial for several metabolic outcomes[20-23], strongly
68 suggesting that TMA and TMAO have distinct biological roles.
69 Here, we present a new paradigm to decipher the microbiome–host kinome chemical
70 crosstalk in IR: i) identification of gut-derived microbial metabolites associated with HFD-
71 induced IGT and obesity, ii) systematic pharmacological target screening of discriminant
72 microbial metabolites, iii) molecular modelling of the interaction, and iv) mechanistic
73 validation of the pathophysiological relevance of pharmacological interactions with *in vivo*
74 models, thereby unravelling novel mechanisms by which gut microbial TMA acts as an IRAK-
75 4 inhibitor and directly improves the host's immunometabolism.
76
77 **Longitudinal study leading to the choline supplementation hypothesis.**
78 We initially carried out a longitudinal pathophysiological monitoring in a cohort of C57BL/6
79 mice (n=472) rapidly developing obesity and IGT when fed a 65% kCal HFD (**Suppl. Fig. 1a-c**).
80 Liver transcriptomics identified 1,641 significant differentially expressed genes between
81 chow-fed (CHD-) and HFD-fed mice (**Suppl. Fig. 1d,e** and **Suppl. Tab. 1**). Gene ontology and
82 signalling pathway impact analyses (**Suppl. Fig. 2, Suppl. Tab. 2-4**) demonstrated
83 upregulation of protein processing in the endoplasmic reticulum, whereas carbohydrate
84 metabolism, circadian rhythm and AMPK signalling were significantly inhibited, consistent
85 with existing literature[24,25]. Surprisingly, inflammation-associated pathways were not
86 differentially affected: expression of genes coding for acute phase serum amyloid A proteins
87 *Saa1* and *Saa2* in response to acute inflammation and associated with type 2 diabetes was
88 reduced whereas expression of pro-inflammatory cytokines such as *Il6* and *Il1β* was not
89 significant (**Suppl. Fig. 1d** and **Suppl. Tab. 4**). This is contrasting with established knowledge
90 as low-grade inflammation is one of the key features associated with IR[4,5]. Metabolic
91 profiling of the urinary metabolome of this mouse cohort (CHD and HFD, 4 time-points) by

92 ^{1}H-NMR spectroscopy followed by multivariate modelling showed diet is the main factor
93 influencing the metabolic profiles, followed by age (**Suppl. Fig. 1f**), the model's goodness-of-
94 prediction parameters being highly significant upon permutation testing (**Suppl. Fig. 1g**).
95 The metabolic signature of HFD-feeding compared to CHD was mainly associated with TMA
96 excretion (**Suppl. Fig. 1h**), consistent with our previous reports using this diet[12,26]. We used
97 variance components analysis to decompose the contribution of diet and age to the
98 excretion of these three metabolites, showing that the HFD contribution overwhelms the
99 contribution of age (**Suppl. Fig. 1i**). Since the HFD contains >15 g of choline per kg of diet,
100 this led us to hypothesize that choline supplementation may explain some of the metabolic
101 and immune variation in response to the HFD.
102
103 **Choline supplementation corrects HFD-induced inflammation and IR.**
104 To investigate the effect of choline supplementation on glucose tolerance and IR, we
105 initiated a series of *in vivo*, *in vitro* and *in silico* studies. We first fed C57BL/6 mice with a
106 65% kCal HFD containing 2 g/kg or 17 g/kg of choline (i.e., LC-HFD and HC-HFD, respectively;
107 **Fig. 1**). Body weight (BW) was significantly increased in mice fed a LC-HFD from weaning
108 until 5 months of age compared to mice fed a chow diet and remarkably compared to mice
109 fed HC-HFD (**Fig. 1a**), which was not related to food intake (**Suppl. Fig. 3a**). To evaluate
110 metabolic homeostasis, we performed glucose tolerance tests (GTT), which displayed a
111 similar pattern with normalisation of cumulative glycemia on HC-HFD compared to LC-HFD
112 (**Fig. 1b-c**). We then profiled circulating pro-inflammatory cytokines such as IL6, IL1β, TNFα
113 (**Fig. 1d-f**) and phosphorylation of NF-κB regulating their transcription (**Suppl. Fig. 3b,c**),
114 which was also suggestive of an improvement of HFD-induced inflammation by choline
115 supplementation.
116
117 **Targeted analysis of choline and methylamine pathways.**
118 To document the effect of choline supplementation on choline-related metabolic pathways,
119 we further refined our isotopic UPLC-MS/MS quantification[27,28] to evaluate plasma
120 concentrations of choline- and carnitine-derived metabolites leading to TMA and TMAO
121 (**Suppl. Fig. 3d,e**). An O-PLS-DA model significantly segregates the three treatment groups at
122 5 months and highlights a choline supplementation effect on the first predictive component
123 (**Fig. 1g,h**). Quantifications all reflect an increase in TMA and TMAO in the HC-HFD in line

124 with choline supplementation (**Fig. 1i,j**). In particular, the circulating TMA levels were similar
125 in the CHD and the LC-HFD (0.38 µM in CHD vs. 0.3 µM in LC-HFD) which was about 20 times
126 less than in the HC-HFD (5.9 µM). These results depict an increased microbial conversion of
127 choline into TMA in our HC-HFD, an observation already made in a previous study[12]. These
128 results suggest that TMA could mediate the metabolic and immune benefits of choline
129 supplementation.
130
131 **Baseline metabolic phenotyping after 2-month HFD feeding.**
132 To further assess the impact of choline supplementation on metabolic homeostasis and low-
133 grade inflammation in HFD contexts, we performed a second experiment, feeding C57BL/6
134 mice a 60% kcal HFD with a time-frame comparable to the ones used in subsequent figures.
135 Weekly BWs and the GTT showed a similar trend after 8 weeks of HFD-feeding (**Fig. 2a-c**).
136 Choline supplementation not only improved glucose tolerance (**Fig. 2b,c**) but also the
137 Matsuda index (**Fig. 2d**), a surrogate marker for IR[29]. The normalisation of insulin sensitivity
138 was confirmed through insulin tolerance tests (ITT) and hepatic Akt phosphorylation assays
139 (**Fig. 2e-h**). We further characterized that HFD feeding increased hepatic NF-κB
140 phosphorylation compared to CHD, which was normalised by choline supplementation (**Fig.
141 2i,j**), a pattern that was also observed for expression of acute-phase proteins *Saa1*, *Saa2*
142 and *Saa3* (**Fig. 2k-m**).
143
144 **Chemical blockage of bacterial TMA biosynthesis and loss of metabolic benefits.**
145 To test whether the beneficial effects of choline supplementation are mediated by its
146 microbial product TMA, we sought to block bacterial TMA production in HC-HFD-fed mice
147 both non-specifically and specifically using, respectively, a wide-spectrum antibiotics
148 cocktail and 3,3-dimethyl-1-butanol (DMB), which inhibits microbial TMA-lyase[30]. We first
149 confirmed the functional blockage of TMA production in mice fed a HC-HFD, resulting in a
150 drastic drop in circulating and excreted TMA and TMAO following 1% DMB administration
151 (**Suppl. Fig. 4a-d)**. In accordance with our hypothesis, both antibiotics and DMB treatments
152 abolished the effects of choline supplementation-induced improvements in HFD, in
153 particular for glucose tolerance, insulin sensitivity (as suggested by the Matsuda index, **Fig.
154 3a-c**, **Suppl. Fig. 4e,f**) and hepatic insulin sensitivity as shown by the absence of beneficial
155 effect of choline supplementation on insulin-induced Akt phosphorylation (**Fig. 3d-g**). The

156 metabolic improvements were not associated with change in BW gain (**Suppl. Fig. 4e**),
157 thereby strongly suggesting that the effects on glucose metabolism induced by inhibiting
158 bacterial TMA production in HC-HFD were decoupled from obesity.
159
160 **TMA treatment mimics choline supplementation.**
161 To further confirm whether TMA mediates the beneficial effects of choline
162 supplementation, we chronically treated LC-HFD-fed C57BL/6 mice with TMA for 6 weeks
163 using subcutaneous osmotic minipumps and assessed their immunometabolism. We
164 confirmed that chronic TMA treatment at 0.01 mM in a LC-HFD did not affect BW gain
165 (**Suppl. Fig. 4g**) but effectively normalised glucose homeostasis and insulin sensitivity (**Fig.**
166 **3h-l, Suppl. Fig. 4d**). TMA treatment also improved the pro-inflammatory response to HFD-
167 feeding and hepatic expression of acute phase proteins *Saa1*, *Saa2* and *Saa3* (**Fig. 3m-p)**.
168 These results suggest that chronic TMA treatment decouples BW gain and adiposity from
169 low-grade inflammation and glucose homeostasis, thereby mimicking the immune and
170 metabolic benefits observed in choline supplementation.
171
172 **TMA is a specific IRAK-4 inhibitor.**
173 To identify a direct mechanism linking TMA to metabolic and immune benefits in HFD-fed
174 mice, we sought to identify its host pharmacological targets. The kinome, made of 518
175 kinases encoded the human genome[6], represents a repertoire of critical signal transduction
176 switches for metabolic homeostasis and inflammation. To discover physical interactions, we
177 screened TMA against a panel of 456 clinically-relevant human kinases using a high-
178 throughput assay[31,32] and identified five preliminary hits for TMA (**Fig. 4a** and
179 **Supplementary Tab. 5**). We then generated multiple-dose binding curves between TMA and
180 each hit and confirmed that only TMA specifically binds IRAK-4 (dissociation constant K_d = 14
181 nM, **Fig. 4b**) whereas TMA did not bind the other four preliminary hits (flat dissociation
182 curves with no K_d fit in **Supplementary Fig. 5a-d**, meaning no physical binding was
183 observed). Since K_d only addresses a physical interaction in its simplest form (*i.e.* binding),
184 we functionally tested TMA as an IRAK-4 inhibitor, by quantifying IRAK-4 phosphorylation
185 activity in presence of ATP and increasing doses of TMA to derive a half-maximal relative
186 inhibitory constant (IC_{50} = 3.4 µM, **Fig. 4c**). We also confirmed that choline, TMAO and DMB
187 do not inhibit IRAK-4 (**Suppl. Fig. 5e-g**) and that TMA does not inhibit IRAK-1 either (**Suppl.**

188 **Fig. 5h**), as *Irak-1*$^{-/-}$ mice fed a HFD were recently shown to have metabolic improvements
189 similar to TMA treatment[33]. Molecular dynamics simulations of IRAK-4 were performed in
190 the presence of 1% TMA. *In silico* analysis of thousands of binding and unbinding events
191 suggests that in solution TMA binds to several small hydrophobic cavities in IRAK-4 and to
192 the ATP binding site (**Fig. 4d** and **Suppl. Fig. 5i-j**).
193 Since IRAK-4 is a central kinase in the TLR pathway sensing bacterial invasion and promoting
194 a pyretic pro-inflammatory response in infectious contexts[34,35], we sought to test its
195 inhibition in a HFD context. The main free fatty acid (FFA) in our HFD is palmitate, a
196 saturated FFA which triggers TLR4. We therefore developed a palmitate-activated Kupffer
197 cell model of HFD-induced low-grade inflammation based on murine KUP5 cell line[36] (**Suppl.**
198 **Fig. 4k**). Palmitate treatment in KUP5 cells significantly increased both IL-6 and TNFα
199 secretions, which were improved by co-treatment with 0.1 mM TMA (**Fig. 4e,f**). Our results
200 reveal that TMA is a specific IRAK-4 inhibitor blunting the palmitate-induced low-grade
201 inflammation *in vitro*, requiring further assessment in Irak4$^{-/-}$ mice.
202
203 ***Irak4*$^{-/-}$ mice are protected against HFD-induced immune and metabolic dysregulations.**
204 IRAK-4 is a key kinase required for defence against pyogenic infections in acute contexts[34,35].
205 To test whether this kinase plays a role in HFD-induced chronic low-grade inflammation and
206 glucose homeostasis, we fed 5-week-old *Irak4*$^{-/-}$ mice[37] and wild-type (WT) littermates in
207 C57BL/6 background a LC-HFD, to avoid potential confounding effects from TMA for 8
208 weeks before assessing circulating cytokines, expression of hepatic inflammatory genes and
209 acute-phase markers and metabolic homeostasis (**Fig. 5a-h**). *Irak4*$^{-/-}$ mice presented
210 improved glycemic control compared to WT littermates (**Fig.5 a,b**). Likewise, the
211 inflammatory response to LC-HFD observed in WT was obliterated in *Irak4*$^{-/-}$ littermates (**Fig.**
212 **5c-g**). There was a similar trend for *Saa3* (**Fig. 5h**), whilst there was no effect on BW gains
213 (**Supplementary Fig. 6a**). Hence, genetic ablation of IRAK-4 abolishes the HFD-induced pro-
214 inflammatory response and IGT thereby decoupling obesity from impaired glucose tolerance
215 and low-grade inflammation with a similar phenotype to *Irak1* deficiency[33].
216
217 **Pharmacological inhibition of Irak4 normalises metabolism.**
218 Since the *Irak4*$^{-/-}$ mice lack the whole protein, we compared the knock-out phenotype with
219 the phenotype of PF06650833, a recently discovered chemical inhibitor of the human IRAK4

220 protein[38] currently being assessed in a clinical trial (NCT02996500). Treatment with
221 PF06650833 improved BW in LC-HFD mice (**Suppl. Fig. 6b**). This inhibitor also yielded
222 significant improvements in plasma glycemia at the latter time-points of the GTT and ITT
223 and in cumulative glycemia (**Fig. 5i-l**), which was mirrored by an increase in Akt
224 phosphorylation (**Fig. 5m-n**). These results collectively show that specific chemical inhibition
225 of IRAK-4 leads to significant improvements in glycemic control, insulin sensitivity and
226 insulin signalling. Further, they suggest that IRAK-4 could constitute a clinically relevant
227 target in IR and related disorders.
228
229
230 **DISCUSSION**
231 The discovery that TMA is a kinase inhibitor controlling IRAK-4, a central kinase involved in
232 innate immunity, is a major finding which provides an attractive mechanism for the
233 metabolic and immune improvements observed with choline-supplementation in HFD
234 contexts (**Fig. 6**).
235 IRAK-4 is the first regulatory checkpoint after MyD88, the adapter protein connecting IRAK-4
236 to at least six TLRs sensing bacterial compounds[39]. IRAK-4 deficiency is associated with
237 bacterial infections in humans[35] and in mice[40]. Consistent with the involvement of the TLR
238 signalling pathway at the crossroads between gut microbiota and dietary lipids[41,42], IRAK-4
239 deletion and its inhibition by TMA and PF06650833[38] rescued HFD-induced low-grade
240 inflammation and IR[4,43,44], highlighting new unexpected roles for this microbial metabolite
241 and its target kinase in immunometabolism. The relative IC_{50} (3.4 µM) we determined is two
242 times smaller than the plasma isotopic quantifications obtained by UPLC-MS/MS in the HFD
243 group supplemented with choline. These quantifications are comparable to circulating TMA
244 levels previously reported in normal human plasma, ranging between 0.42 and 48 µM[45,46],
245 which makes this IC_{50} particularly relevant with regard to pathophysiological mechanisms:
246 dosing mice with 0.01 mM TMA (3x IC_{50}) was sufficient to improve inflammatory and
247 metabolic responses. TMA can therefore be considered a "microbial signalling metabolite"[47]
248 sending a negative feedback signal to a pathway triggered by influx of saturated free fatty
249 acids in HFD contexts, this mechanism participating in maintaining a low immunological
250 footprint and metabolic improvements in a symbiotic relationship. TMA's role as an IRAK-4
251 inhibitor could for instance explain some of the beneficial effects reported for choline

252 supplementation in NAFLD patients[48]. Altogether, our results on IRAK-4 inhibition and
253 ablation provide further insight in the phenotypic convergence between *Myd88*, *Irak4* and
254 *Irak1* knock-out mouse models[33,49], suggesting that the gut microbiota, through TMA,
255 proceeds with a targeted hijacking of the TLR signal transduction machinery to the host's
256 benefit resulting in metabolic and immune improvements.
257 In summary, through the combination of *in silico*, *ex vivo*, *in vitro* and *in vivo* approaches, we
258 reveal a unique mechanism in which TMA acts as a gut microbial signalling metabolite
259 inhibiting IRAK-4, a central molecular target in the TLR pathway, thereby allowing the gut
260 microbiota to control HFD-induced pro-inflammatory response and IR. The kinome
261 represents a key repertoire of regulatory host targets for microbial signals and the
262 uncharted microbiome–kinome crosstalk requires further investigation. By highlighting the
263 physiological and therapeutic roles of TMA and IRAK-4 on HFD-induced low-grade
264 inflammation and IR, we anticipate that its immunomodulatory properties extend beyond IR
265 to a wider range of human pathologies involving TLR signalling and modulation of innate
266 immunity.
267

268 **Author Contributions**

269 JC and SG performed cell-based assays, JC performed multivariate statistics and interpreted
270 the results. JC, FB, JFF, AE, HP, LZ, DS, ARR, PDC, SC and CG contributed *in vivo* experiments,
271 RHB, AM, ALN, LMG, SG, CLB and SP performed various experiments. JEF and RCG designed
272 and performed *in silico* experiments. LH analysed microarray data. JS, DG, JKN, PPL, PDC,
273 NJG and MED conceived the project, mentored and supervised its participants and
274 interpreted its results. MED performed metabolic profiling experiments, analysed data and
275 interpreted the results. JC, NJG, DG, PPL, PDC, and MED wrote the manuscript. All authors
276 edited the manuscript.

277

278 **Acknowledgments**

279 This work was supported by grants from the Wellcome Trust (Functional Genomics Initiative
280 grant Biological Atlas of Insulin Resistance 06678 to JKN, DG and JS), the European
281 Commission (METACARDIS HEALTH-F4-2012-305312 to DG and MED, Neuron II under
282 agreement 291840 and the MRC (MR/M501797/1 to MED), Institut Mérieux through a grant
283 awarded to MED, and Canadian Institutes of Health Research (CIHR) grants (MOP-49413 &
284 MOP-142471) awarded to PPL. DG held a Wellcome Trust Senior Fellowship in Basic
285 Biomedical Science (057733). JEF was supported by the Medical Research Council (grant
286 number MR/K020919/1). PDC is a senior research associate and AE a research associate at
287 FRS-FNRS (Fonds de la Recherche Scientifique). PDC is the recipient of grants from FNRS. LH
288 is in receipt of an MRC Intermediate Research Fellowship in Data Science (grant number
289 MR/L01632X/1, UK Med-Bio). This work was supported by FRFS-WELBIO under grant:
290 WELBIO-CGR-2017, by the Funds InBev-Baillet Latour (Grant for Medical Research 2015) and
291 ERC Starting Grant 2013 (European Research Council, Starting grant 336452-ENIGMO).

292

293 **Online Content.**

294 Methods, along with any additional Supplementary display items and Source Data, are
295 available in the online version of the paper; references unique to these sections appear only
296 in the online paper.

297 **References.**

298 1. Wu, G. D. *et al.* Linking long-term dietary patterns with gut microbial enterotypes.
299 *Science* **334,** 105–108 (2011).
300 2. Le Chatelier, E. *et al.* Richness of human gut microbiome correlates with metabolic
301 markers. *Nature* **500,** 541–546 (2013).
302 3. Pedersen, H. K. *et al.* Human gut microbes impact host serum metabolome and
303 insulin sensitivity. *Nature* **535,** 376–381 (2016).
304 4. Cai, D. *et al.* Local and systemic insulin resistance resulting from hepatic activation of
305 IKK-beta and NF-kappaB. *Nat. Med.* **11,** 183–190 (2005).
306 5. Cani, P. D. *et al.* Metabolic endotoxemia initiates obesity and insulin resistance.
307 *Diabetes* **56,** 1761–1772 (2007).
308 6. Manning, G., Whyte, D. B., Martinez, R., Hunter, T. & Sudarsanam, S. The protein
309 kinase complement of the human genome. *Science* **298,** 1912–1934 (2002).
310 7. Samuel, V. T. & Shulman, G. I. Mechanisms for insulin resistance: common threads
311 and missing links. *Cell* **148,** 852–871 (2012).
312 8. Hooper, L. V., Littman, D. R. & Macpherson, A. J. Interactions between the microbiota
313 and the immune system. *Science* **336,** 1268–1273 (2012).
314 9. Nicholson, J. K. *et al.* Host-gut microbiota metabolic interactions. *Science* **336,** 1262–
315 1267 (2012).
316 10. Maslowski, K. M. *et al.* Regulation of inflammatory responses by gut microbiota and
317 chemoattractant receptor GPR43. *Nature* **461,** 1282–1286 (2009).
318 11. Venkatesh, M. *et al.* Symbiotic Bacterial Metabolites Regulate Gastrointestinal Barrier
319 Function via the Xenobiotic Sensor PXR and Toll-like Receptor 4. *Immunity* **41,** 296–
320 310 (2014).
321 12. Dumas, M.-E. *et al.* Metabolic profiling reveals a contribution of gut microbiota to
322 fatty liver phenotype in insulin-resistant mice. *Proc. Natl. Acad. Sci. U.S.A.* **103,**
323 12511–12516 (2006).
324 13. Wang, Z. *et al.* Gut flora metabolism of phosphatidylcholine promotes cardiovascular
325 disease. *Nature* **472,** 57–63 (2011).
326 14. Al-Waiz, M., Mikov, M., Mitchell, S. C. & Smith, R. L. The exogenous origin of
327 trimethylamine in the mouse. *Metab. Clin. Exp.* **41,** 135–136 (1992).
328 15. Craciun, S. & Balskus, E. P. Microbial conversion of choline to trimethylamine requires
329 a glycyl radical enzyme. *Proc. Natl. Acad. Sci. U.S.A.* **109,** 21307–21312 (2012).
330 16. Koeth, R. A. *et al.* Intestinal microbiota metabolism of L-carnitine, a nutrient in red
331 meat, promotes atherosclerosis. *Nat. Med.* **19,** 576–585 (2013).
332 17. Al-Waiz, M., Ayesh, R., Mitchell, S. C., Idle, J. R. & Smith, R. L. Disclosure of the
333 metabolic retroversion of trimethylamine *N*-oxide in humans: a pharmacogenetic
334 approach. *Clin. Pharmacol. Ther.* **42,** 608–612 (1987).
335 18. Hoyles, L. *et al.* Metabolic retroconversion of trimethylamine *N*-oxide and the gut
336 microbiota. *bioRxiv* 225581 (2017). doi:10.1101/225581
337 19. Dolphin, C. T., Janmohamed, A., Smith, R. L., Shephard, E. A. & Phillips, I. R. Missense
338 mutation in flavin-containing mono-oxygenase 3 gene, FMO3, underlies fish-odour
339 syndrome. *Nat. Genet.* **17,** 491–494 (1997).
340 20. Shih, D. M. *et al.* Flavin containing monooxygenase 3 exerts broad effects on glucose
341 and lipid metabolism and atherosclerosis. *J. Lipid Res.* **56,** 22–37 (2015).
342 21. Warrier, M. *et al.* The TMAO-Generating Enzyme Flavin Monooxygenase 3 Is a Central
343 Regulator of Cholesterol Balance. *Cell Rep* **10,** 326–338 (2015).

344 22. Miao, J. *et al.* Flavin-containing monooxygenase 3 as a potential player in diabetes-
345 associated atherosclerosis. *Nat Commun* **6,** 6498 (2015).
346 23. Schugar, R. C. *et al.* The TMAO-Producing Enzyme Flavin-Containing Monooxygenase
347 3 Regulates Obesity and the Beiging of White Adipose Tissue. *Cell Rep* **19,** 2451–2461
348 (2017).
349 24. Ozcan, U. *et al.* Endoplasmic reticulum stress links obesity, insulin action, and type 2
350 diabetes. *Science* **306,** 457–461 (2004).
351 25. Eckel-Mahan, K. L. *et al.* Reprogramming of the circadian clock by nutritional
352 challenge. *Cell* **155,** 1464–1478 (2013).
353 26. Dumas, M.-E. *et al.* Microbial-Host Co-metabolites Are Prodromal Markers Predicting
354 Phenotypic Heterogeneity in Behavior, Obesity, and Impaired Glucose Tolerance. *Cell*
355 *Rep* **20,** 136–148 (2017).
356 27. Kadar, H. *et al.* A multiplexed targeted assay for high-throughput quantitative analysis
357 of serum methylamines by ultra performance liquid chromatography coupled to high
358 resolution mass spectrometry. *Arch. Biochem. Biophys.* **597,** 12–20 (2016).
359 28. Plovier, H. *et al.* A purified membrane protein from Akkermansia muciniphila or the
360 pasteurized bacterium improves metabolism in obese and diabetic mice. *Nat. Med.*
361 **23,** 107–113 (2017).
362 29. Matsuda, M. & DeFronzo, R. A. Insulin sensitivity indices obtained from oral glucose
363 tolerance testing: comparison with the euglycemic insulin clamp. *Diabetes Care* **22,**
364 1462–1470 (1999).
365 30. Wang, Z. *et al.* Non-lethal Inhibition of Gut Microbial Trimethylamine Production for
366 the Treatment of Atherosclerosis. *Cell* **163,** 1585–1595 (2015).
367 31. Fabian, M. A. *et al.* A small molecule-kinase interaction map for clinical kinase
368 inhibitors. *Nat. Biotechnol.* **23,** 329–336 (2005).
369 32. Karaman, M. W. *et al.* A quantitative analysis of kinase inhibitor selectivity. *Nat.*
370 *Biotechnol.* **26,** 127–132 (2008).
371 33. Sun, X.-J. *et al.* Deletion of interleukin 1 receptor-associated kinase 1 (Irak1) improves
372 glucose tolerance primarily by increasing insulin sensitivity in skeletal muscle. *J. Biol.*
373 *Chem.* **292,** 12339–12350 (2017).
374 34. Suzuki, N. *et al.* Severe impairment of interleukin-1 and Toll-like receptor signalling in
375 mice lacking IRAK-4. *Nature* **416,** 750–756 (2002).
376 35. Picard, C. *et al.* Pyogenic bacterial infections in humans with IRAK-4 deficiency.
377 *Science* **299,** 2076–2079 (2003).
378 36. Kitani, H. *et al.* Establishment of c-myc-immortalized Kupffer cell line from a C57BL/6
379 mouse strain. *Results Immunol* **4,** 68–74 (2014).
380 37. Valaperti, A. *et al.* Innate immune interleukin-1 receptor-associated kinase 4
381 exacerbates viral myocarditis by reducing CCR5(+) CD11b(+) monocyte migration and
382 impairing interferon production. *Circulation* **128,** 1542–1554 (2013).
383 38. Lee, K. L. *et al.* Discovery of Clinical Candidate 1-{[(2S,3S,4S)-3-Ethyl-4-fluoro-5-
384 oxopyrrolidin-2-yl]methoxy}-7-methoxyisoquinoline-6-carboxamide (PF-06650833), a
385 Potent, Selective Inhibitor of Interleukin-1 Receptor Associated Kinase 4 (IRAK4), by
386 Fragment-Based Drug Design. *J. Med. Chem.* **60,** 5521–5542 (2017).
387 39. O'Neill, L. A. J., Golenbock, D. & Bowie, A. G. The history of Toll-like receptors -
388 redefining innate immunity. *Nat. Rev. Immunol.* **13,** 453–460 (2013).
389 40. Bernuth, von, H., Picard, C., Puel, A. & Casanova, J.-L. Experimental and natural
390 infections in MyD88- and IRAK-4-deficient mice and humans. *Eur. J. Immunol.* **42,**

3126–3135 (2012).
41. Caesar, R., Tremaroli, V., Kovatcheva-Datchary, P., Cani, P. D. & Backhed, F. Crosstalk between Gut Microbiota and Dietary Lipids Aggravates WAT Inflammation through TLR Signaling. *Cell Metab.* **22,** 658–668 (2015).
42. Shi, H. *et al.* TLR4 links innate immunity and fatty acid-induced insulin resistance. *J. Clin. Invest.* **116,** 3015–3025 (2006).
43. Reilly, S. M. *et al.* An inhibitor of the protein kinases TBK1 and IKK-β improves obesity-related metabolic dysfunctions in mice. *Nat. Med.* **19,** 313–321 (2013).
44. Kiechl, S. *et al.* Blockade of receptor activator of nuclear factor-κB (RANKL) signaling improves hepatic insulin resistance and prevents development of diabetes mellitus. *Nat. Med.* **19,** 358–363 (2013).
45. Bain, M. A., Faull, R., Fornasini, G., Milne, R. W. & Evans, A. M. Accumulation of trimethylamine and trimethylamine-N-oxide in end-stage renal disease patients undergoing haemodialysis. *Nephrol. Dial. Transplant.* **21,** 1300–1304 (2006).
46. Lundh, T., Akesson, B. & Skerfving, S. Effect of dietary intake of trimethylamine on human metabolism of the industrial catalyst dimethylethylamine. *Occup Environ Med* **52,** 478–483 (1995).
47. Dumas, M.-E. The microbial-mammalian metabolic axis: beyond simple metabolism. *Cell Metab.* **13,** 489–490 (2011).
48. Spencer, M. D. *et al*. Association between composition of the human gastrointestinal microbiome and development of fatty liver with choline deficiency. *Gastroenterology* **140,** 976–986 (2011).
49. Everard, A. *et al.* Intestinal epithelial MyD88 is a sensor switching host metabolism towards obesity according to nutritional status. *Nat Commun* **5,** 5648 (2014).

416 **Online Methods**

417 **Protocols**

418 All experimental procedures involving mice were carried out in accordance with U.K. Home
419 Office, Canadian Council on Animal Care, the ethics committee of the French Research
420 Ministry (authorization number 00486.01), Belgian Law of May 29, 2013 regarding the
421 protection of laboratory animals (agreement number LA1230314) and local guidelines on
422 animal welfare and license conditions and the University of Oxford, University of Ottawa,
423 Université Pierre et Marie Curie and Université Catholique de Louvain guidelines on animal
424 welfare.

425

426 **Cell-based assays.**

427 C-myc-immortalised KUP5 cells, originally harvested from a C57BL/6 mouse, were
428 purchased from RIKEN BioResource Center, which certified the cells were not contaminated
429 by *Mycoplasma*. They were cultured in splitting medium at 37°C and 5% CO_2 atmosphere
430 under sterile conditions. Cells were split every 48-72 h using splitting medium (DMEM
431 GlutaMAX-I supplemented with 10% FBS, 1% penicillin and streptomycin, 0.1% insulin and
432 0.044% thioglycerol), maintained at a density between $5 \times 10^5 - 1 \times 10^6$ cells/mL and used
433 between passages 2 and 20. For palmitate (PA) treatment, 125,000 cells/cm^2 were seeded in
434 treatment medium (DMEM GlutaMAX-I supplemented with 5% FBS, 1% penicillin and
435 streptomycin, 0.1% insulin and 0.044% thioglycerol) on a 48-well plate with a working
436 volume of 250 µL and incubated at 37°C and 5% CO_2 atmosphere overnight (16-18 h). 0.5 M
437 PA stock solution was prepared in 100% ethanol and 0.5 mM PA treatment solution was
438 prepared in treatment medium containing a final concentration of 0.5% low-endotoxin-fatty
439 acid free BSA. TMA (0.1 mM) treatment was performed in a simultaneous fashion with PA.
440 All solutions containing PA were prepared in borosilicate glass tubes. Upon overnight
441 incubation of seeded cells, the medium was replaced with the same volume of treatment
442 solutions and incubated at 37°C and 5% CO_2 atmosphere for 24 h before measurement of
443 cytokines in the medium.

444

445 **Mouse Models.**

446 Longitudinal HFD-feeding in mice**.** All experiments were approved by the ethical committee
447 of the University of Oxford. Male mice from C57BL/6J inbred strain were bred in our animal

448 facility by using a stock originating from The Jackson Laboratory. At 5 weeks of age, groups
449 of n=8-10 mice were transferred to a 40 %w/w high fat diet (65% kcal) (Special Diets
450 Services), containing 32 % lard and 8 % corn oil, whereas control groups remained on a 5 %
451 Low Fat Diet (B & K Universal) for up to 6 months. Detailed diet formulations were
452 published previously[12] and summarised in **Supplementary Table 6**.
453
454 Mice were housed under a 12 h–12 h light–dark cycle. For physiological profiling, several
455 mouse groups fed CHD or HFD were tested to assess consistency of results and discard any
456 impact of potential batch effects. Intra peritoneal glucose tolerance tests (ipGTT) were
457 performed in mice after 2-, 3-, 5-and 7-month-old mice after an overnight fast, as previously
458 published[50] (see also metabolic phenotyping below). Four days after the GTT, 24 h urinary
459 samples (9 a.m. to 9 a.m.) were collected from mice maintained in individual metabolic
460 cages. Urinary samples collected in a solution of 1 % (wt/vol) sodium azide were centrifuged
461 to remove solid particles and kept at -80°C until assayed. After an overnight fast, mice were
462 killed by exsanguination. Plasma was separated by centrifugation and stored at -80 °C until
463 ^{1}H-NMR analysis.
464
465 *Choline supplementation on HFD.* At 5 weeks of age, mice were fed either a chow diet
466 containing 2g of choline/kg of diet (Research Diets, D12450J), a low-choline HFD containing
467 2g of choline/kg of diet (Research diets, D12492), a high-choline HFD containing 17 g of
468 choline/kg of diet (Research diets, D16100401), a HC-HFD containing 1% of DMB or a HC-
469 HFD combined with a cocktail of antibiotics (0.5 g/L vancomycin hydrochloride, 1 g/L
470 neomycin trisulfate, 1 g/L metronidazole, 1 g/L ampicillin sodium) in drinking bottles (n=6-
471 10 per group) for 8 weeks (see diet formulations in **Supplementary Table 6**). Mice then
472 were killed by decapitation and organ were dissected and weighed.
473
474 *Irak4*$^{-/-}$ mice. *Irak4*$^{-/-}$ mice on C57BL/6J background as already described[37] were bred with
475 C57BL/6J female mice (The Jackson Laboratory), and the F1 offspring were subsequently
476 bred to produce *Irak4*$^{-/-}$ mice and WT littermate used for this study. After eight weeks of
477 HFD-feeding, mice were killed by decapitation and organ were dissected and weighed.
478

479 *Chronic TMA and PF06650833 treatment in LC-HFD-fed mice.* Five-week-old C57BL/6J mice
480 (Charles River) were housed a week before experiment in a controlled environment. Mice
481 were housed under a 12 h–12 h light–dark cycle. At day 0, the 10-week-old mice were
482 anaesthetised with isoflurane (ForeneH, Abbott). Mini-osmotic pumps were implanted
483 subcutaneously (Model 2006, Alzet) (flow rate: 0.15 mL/h, total filling volume: 200 mL,
484 delivery duration: 42 days) as previously described[51]. The osmotic mini-pump contains
485 either vehicle or TMA (0.1 mM in circulation) or PF06650833 (50 nM in circulation). After six
486 weeks of metabolite treatment, mice were killed by decapitation and organ were dissected
487 and weighed.
488
489 **Physiological phenotyping**
490 After four weeks of treatment an intra-peritoneal glucose tolerance test (2g/kg) was
491 performed in conscious mice following an overnight fast. Blood was collected from the tail
492 vein before glucose injection and 30, 60, 90 and 120 minutes afterwards. Blood glucose
493 levels were determined using an Accu-Check® Performa (Roche Diagnostics, Meylan,
494 France). Additional blood samples were collected at baseline and 30 minutes after glucose
495 injection in Microvette® CB 300 Lithium Heparin (Sarstedt, Marnay, France). Plasma was
496 separated by centrifugation and stored at -80°C until insulin radioimmunoassay. Circulating
497 insulin levels were determined using Insulin ELISA kits (Mercodia, Uppsala, Sweden). The
498 Matsuda insulin sensitivity index was calculated as previously published[29].
499 After five weeks, we performed an insulin tolerance test. 5 hour-fasted mice were injected
500 intraperitoneally with insulin (0.75 mU/g, Actrapid, Novo Nordisk). Blood glucose levels
501 were measured immediately before and 15, 30, 45, 60, 90 and 120 min after insulin
502 injection with a standard glucose meter (Accu Check, Roche, Basel, Switzerland) on the tip
503 of the tail vein.
504
505 **Gene expression.**
506 Groups of 6 mice showing consistent pathophysiological profile in response to CHD or HFD
507 treatment were selected for microarray analysis performed as previously described[52] and
508 data were deposited in array express with accession number: E-MEXP-1755. The
509 Bioconductor[53] package Limma[54] was used to generate the list of differentially expressed

510 genes. Gene ontology was implemented using Enrichr[55] and signalling pathway impact
511 analysis using SPIA[56].
512 For qPCR analysis, total RNA was prepared from tissues using TriPure reagent (Roche).
513 Quantification and integrity analysis of total RNA were performed by analysing 1 µL of each
514 sample in an Agilent 2100 Bioanalyzer (Agilent RNA 6000 Nano Kit, Agilent). cDNA was
515 prepared by reverse transcription of 1 mg total RNA using a Reverse Transcription System
516 kit (Promega). Real-time PCR was performed with the StepOnePlus real-time PCR system
517 and software (Applied Biosystems) using Mesa Fast qPCR (Eurogentec) for detection
518 according to the manufacturer's instructions. RPL19 RNA was chosen as the housekeeping
519 gene. All samples were performed in duplicate in a single 96-well reaction plate and data
520 were analysed according to the 2_DDCT method. The identity and purity of the amplified
521 product were assessed by melting curve analysis at the end of amplification. The primer
522 sequences for the targeted mouse genes are: SAA1 forward CAT-TTG-TTC-ACG-AGG-CTT-
523 TCC, SAA1 reverse GTT-TTT-CCA-GTT-AGC-TTC-CTT-CAT-GT, SAA2 forward GGG-GTC-TGG-
524 GCT-TCC-CAT-CT, SAA2 reverse CCA-TTC-TGA-AAC-CCT-TGT-GG, SAA3 forward CGC-AGC-
525 ACG-AGC-AGG-AT, SAA3 reverse CCA-GGA-TCA-AGA-TGC-AAA-GAA-TG.Q-RT-PCR assays
526 were performed in a single batch with the personnel blind to treatment groups.
527
528 **Circulating cytokine quantification.**
529 Circulating cytokines were quantified using MSD V-PLEX Plus Proinflammatory Panel 1 kit.
530 Plasma samples were diluted 2 times in diluent 41 provided and experiment was processed
531 as request by manufacturer and read on a SECTOR imager 2400. Cytokine assays were
532 performed in a single batch with the personnel blind to treatment groups.
533
534 **Western-blotting.**
535 Western blot analyses were performed as described previously [28]. To analyze the insulin
536 signaling pathway, mice were allocated to either a saline-injected subgroup or an insulin-
537 injected subgroup so that both subgroups were matched in terms of BW and fat mass. They
538 then received 1 mU insulin/g BW (Actrapid; Novo Nordisk A/S, Denmark) or an equal volume
539 of saline solution. Three minutes after injection, mice were killed and liver was harvested.
540 30mg of liver were homogenized in 680 µL of RIPA buffer containing a cocktail of protease
541 and phosphatase inhibitors. The homogenate was then centrifuged at 12,000G for 20 min at

542 4 °C. Equal amounts of proteins were separated by SDS–PAGE and transferred to
543 nitrocellulose membranes. Membranes were incubated overnight at 4 °C with antibodies
544 diluted in Tris-buffered saline Tween-20 containing 1% bovine serum albumin: p-Akt Ser473
545 (1:1,000; #4060, Cell Signaling), Total Akt (1:1000 ,#9272S, Cell Signalling), p-NF-κB (1:3000,
546 #ab86299, AbCam), Total NF- κB p65 (1:3000, #8242, Cell Signalling).
547
548 **^{1}H-NMR spectroscopy and multivariate statistics.**
549 Mouse urine and plasma samples were prepared and measured on a spectrometer (Bruker)
550 operating at 600.22 MHz ^{1}H frequency; full resolution ^{1}H NMR spectra were then processed
551 and analysed using orthogonal partial least square discriminant analysis as described
552 previously[12]. Variance component analysis was performed as described previously[57]. ^{1}H
553 NMR profiling was performed in a single batch with the personnel blind to treatment
554 groups. The O-PLS-DA model was validated using 10,000 random permutations of the
555 original class membership variable to explain (i.e. diets, treatments or genotypes), as
556 described previously[57].
557
558 **Plasma methylamine quantification by UPLC-MS/MS.** Methylamines were quantified as
559 previously described[27,28]. Plasma samples (20 µL) were spiked with 10 µL Internal Standard
560 (IS) solution ($^{13}C_3$/^{15}N-TMA, d_9-TMAO, d_4-choline, d_3-carnitine and d_9-betaine in water; 1
561 mg/L) and 45 µL of ethyl 2-bromoacetate solution (15 g/L ethyl 2-bromoacetate, 1% NH_4OH
562 in acetonitrile) were added to derivatize methylamines (TMA and $^{13}C_3$/^{15}N-TMA) to their
563 ethoxy- analogues, completed after 30 min at room temperature. 935 µL of protein/lipid
564 precipitation solution (94% acetonitrile/5% water/1% formic acid) was added; samples were
565 centrifuged for 20 min (4°C, 20,000g) and were transferred to UPLC-autosampler vials.
566 Sample injections (10 µL loop) were performed on a Waters Acquity UPLC-Xevo TQ-S UPLC-
567 MS/MS system equipped with an Acquity BEH HILIC (2.1 × 100 mm, 1.7 µm)
568 chromatographic column. An isocratic elution was applied with 10 mM ammonium formate
569 in 95:5 (v/v) acetronitrile:water for 14min at 500 µL/min and 50 °C. Positive electrospray
570 (ESI+) was used as ionization source and mass spectrometer parameters were set as follows:
571 capillary, cone and source offset voltages at 500, 93 and 50 V, respectively, desolvation
572 temperature at 600°C, desolvation/cone/nebulizer gases were high-purity nitrogen at 1000
573 L/hr, 150 L/hr and 7 bar respectively. Collision gas was high-purity argon. Mass

574 spectrometer was operated in multiple reactions monitoring (MRM) mode. The monitored
575 transitions were the following: for derivatized-TMA, +146 -> +118/59 *m/z* (23/27 V); for
576 derivatised-$^{13}C_3$/^{15}N-TMA, +150 -> +63 (27V); for TMAO, +76 -> +59/58 *m/z* (12/13 V); for d_9-
577 TMAO, +85 -> +68 *m/z* (18 V); for choline, +104-> +60/45 *m/z* (14/16 V); for d_4-choline, +108
578 -> +60 *m/z* (15 V); for γ-butyrobetaine, +146 -> +60/87 *m/z* (12/12 V); for carnitine, +162 ->
579 +103/60 *m/z* (16/14 V); for d_3-carnitine, +165 -> +103 *m/z* (16 V); for betaine, +118 ->
580 +59/58 *m/z* (16/16 V); for d_9-betaine, +127 -> +68 *m/z* (16 V).
581
582 **Kinome screen, K_d and IC_{50} determination.**
583 TMA was assessed using KdELECT screening service (DiscoveRx) as described previously[31,32].
584 This technique is based on a competition-binding assay that quantitatively measures the
585 ability of a compound to compete with an immobilized, active site-directed ligand. The
586 assay consists of DNA-tagged kinase, immobilized ligand, and the potent inhibitor. The
587 ability of TMA to compete with the immobilized ligand was measured by quantitative PCR of
588 the DNA tag. The binding constant (K_d) was then calculated from duplicate 11-point dose–
589 response curve. Kinase interaction tree plots were generated using TREEspot™ Software
590 Tool and reprinted with permission from KINOMEscan®, a division of DiscoveRx Corporation,
591 © Discoverx corporation 2015. The TMA IC_{50} on IRAK-4 was determined using Kinexus
592 kinase-inhibitor activity profiling service (Kinexus, Vancouver, Canada). The technique is
593 based on the direct quantification of radiolabelled phosphate from ATP onto a protein
594 substrate of a target protein kinase.
595
596 **Molecular dynamics simulations.**
597 Molecular dynamics simulations were performed within the Amber package[58] based on an
598 X-ray structure of human IRAK-4[59]. After removal of the bound ligand and sulfate ions, the
599 system was prepared using protonate3d[60]. Protein atoms were described using the Amber
600 fore field 99SB-ILDN[61], ligand TMA was described within the Generalized Amber Force
601 Field[62] after fitting partial charges using RESP at the Hartree-Fock/6-31G* level (see
602 Supplementary 2e for resulting parameters). A periodic truncated octahedral shell of TIP3P
603 water molecules was added[63] 10Å to our systems. 1% of approximately 10,000 water
604 molecules with a minimum distance of 4Å to the protein were randomly replaced by TMA to
605 study binding. After applying an elaborate equilibration protocol[64], we sampled each system

606 without restraints for 100 ns using the GPU implementation of pmemd[58]. Analyses of
607 simulation data were performed using ptraj and cpptraj from AmberTools[65]. After
608 performing standard stability checks for energy and overall structure, hydrogen bonding
609 between protein and ligands was counted using cpptraj's default criteria. All protein–ligand
610 contacts within a distance cutoff of 5Å were considered for contact analysis. Grid-based
611 analyses of TMA positions were performed on a grid capturing the entire simulation box
612 with a spacing of 0.5Å. The resulting grids were overlaid with an ATP-bound structure of
613 IRAK-4 (PDB: 2OID)[66].
614
615 **Reagents.**
616 Glutamine (Glutamax, 35050061, Life Technologies), Fetal bovine serum (Life Technologies),
617 crystal violet (C6158) and Trimethylamine (W324108) were from Sigma-Aldrich. Mouse IL-6
618 Quantikine ELISA kits (M6000B, R&D system), RNeasy Micro Kit (Qiagen). SuperScript II
619 Reverse Transcriptase, IL6 Taqman probe Hs00174131_m1 and FAST master mix
620 (Invitrogen). High Fat Diet (Special Diets Services) and Low Fat Diet (B & K Universal) were
621 specifically formulated in[12]. Control Diet (D12450K; Research diet), LC-HFD (60% kcal fat and
622 20% kcal carbohydrates, D12492, Research diet), HC-HFD (60% kcal fat and 20% kcal
623 carbohydrates with 17g of choline/kg, D16100401i, Research diet). Mouse Insulin ELISA (10-
624 1249-01, Mercodia). Isoflurane (10014451, Forene, Abbott). TriPure reagent (1667165,
625 Roche). Reverse Transcription System kit (A3500, Promega). Mesa Fast qPCR (CS-CKIT-PROD,
626 Eurogentec). MSD V-PLEX Plus Proinflammatory Panel 1 kit (K15048G Meso Scale
627 Diagnostics).
628
629 **Statistics.**
630 Potential outliers were identified by a Grubbs test. For statistical comparisons between
631 study groups, normality was tested using D'agostino-Pearson omnibus normality test, then
632 one-way ANOVA was used, followed by Tukey's *post hoc* testing when data were normally
633 distributed, otherwise groups were compared using the two-tailed Mann-Whitney test ($P <$
634 0.05 considered to be statistically significant). Data are displayed as mean ± s.e.m in all
635 figures. All cell culture experiments included at least three biological replicates (as indicated
636 in figure legends). All animal cohorts included at least five animals in each study group (as
637 indicated in figure legends) and animals were randomized to treatment groups.

638 **Figure Legends.**

639

640 **Figure 1. Choline supplementation improves glucose homeostasis and inflammation after**
641 **5 months of HFD.**

642 5-week-old C57BL/6J mice were fed a CHD diet, a low-choline HFD or a low-choline HFD
643 supplemented with choline (n=10) and were phenotyped after 5 months. (**a**) Body weight
644 (BW) measured after 5 months of diet. (**b**) Plasma glucose concentration during an ipGTT.
645 (**c**) Area under the curve of the plasma glucose concentration during an ipGTT. (**d-f**)
646 Quantification of circulating cytokines: IL6 (**d**), TNFα (**e**) and IL1β (**f**). (**g**) Scores plot from a
647 cross-validated O-PLS-DA model segregating the three groups of mice according to diet
648 based on isotopic quantification of methylamines by UPLC-MS/MS. (**h**) Empirical assessment
649 of the significance of O-PLS goodness-of-fit parameters by generating a null distribution with
650 10,000 random permutations. (**i-j**) Quantification of circulating TMA (**i**) and TMAO (**j**) by
651 UPLC-MS/MS. Data are means ± s.e.m. One-way ANOVA followed by Tukey's *post hoc* tests
652 (superscript letters for factor levels $P<0.05$) on log-transformed data except (**g-h**).

653

654 **Figure 2. Choline supplementation corrects HFD adverse effects on glucose homeostasis,**
655 **insulin sensitivity and inflammation after 8 weeks of diet.**

656 5-week-old C57BL/6J mice were fed a CHD diet, a low-choline HFD or a low-choline HFD
657 supplemented with choline (n = 10) and were phenotyped after 8 weeks. (**a**) Body weight
658 measured periodically during 8 weeks of diet. (**b**) Plasma glucose concentration during an
659 ipGTT. (**c**) Area under the curve of the plasma glucose concentration during an ipGTT. (**d**)
660 Matsuda insulin sensitivity index calculated from the ipGTT. (**e**) Plasma glucose
661 concentration during an ipITT. (**f**) Area under the curve of the plasma glucose concentration
662 during an ipITT. (**g-j**) Western-Blot analysis of liver Akt phosphorylation (**g-h**) and NF-kB
663 phosphorylation (**i-j**). (**k-m**) expression of hepatic acute phase inflammation proteins
664 markers *Saa1* (**k**), *Saa2* (**l**) and *Saa3* (**m**). Data are means ± s.e.m. (**c**, **d**, **f**, **h-m**) One-way
665 ANOVA followed by Tukey's *post hoc* tests (superscript letters for factor levels $P<0.05$) on
666 log-transformed data. (**a**, **b**, **e**) Non-parametric two-sided Mann-Whitney test was used for
667 each timepoint, significance comparison signs are as follow: *=CHD vs LC-HFD, $=LC-HFD vs
668 HC-HFD and #=CHD vs HC-HFD.

669

670 **Figure 3. Blocking TMA production from choline cancels metabolic benefits from choline**
671 **supplementation and chronic TMA chronic treatment mimics it.**
672 **(a-g)** 5-weeks-old C57BL/6J mice were fed a low-choline HFD or a low-choline HFD
673 supplemented with choline (n = 10). Two strategies were used in parallel to block TMA
674 production from choline by the gut microbiota using either 1% DMB in the diet or an
675 antibiotic treatment. (**a**) Plasma glucose concentration during an ipGTT. (**b**) Area under the
676 curve of the plasma glucose concentration during an ipGTT. (**c**) Matsuda insulin sensitivity
677 index calculated from the ipGTT (**d**) Plasma glucose concentration during an ipITT. (**e**) Area
678 under the curve of the plasma glucose concentration during an ipITT. (**f-g**) Western-blot
679 analysis of liver Akt phosphorylation. (**h-p**) Mice were weaned at 3 weeks and fed a low-
680 choline HFD before being fitted with osmotic minipumps delivering a chronic circulating
681 dose of TMA (0.1 mM) for 6 weeks (n = 9 saline HFD, n = 8 TMA HFD). (**h**) Plasma glucose
682 concentration during an ipGTT. (**i**) Area under the curve of the plasma glucose concentration
683 during an ipGTT. (**j**) Matsuda insulin sensitivity index calculated from the ipGTT. (**k**) Plasma
684 glucose concentration during an ipITT. (**l**) Area under the curve of the plasma glucose
685 concentration during an ipITT. (**m**) Quantification of circulating IL6. (**n-p**) Expression of
686 hepatic acute-phase inflammation protein markers *Saa1* (**n**), *Saa2* (o) and *Saa3* (**p**). Data are
687 means ± s.e.m. Results were assessed by one-way analysis of variance followed by Tukey's
688 *post hoc* tests (superscript letters for factor levels $P<0.05$) on log-transformed data.
689
690 **Figure 4. TMA inhibits IRAK-4 and rescues TLR4-mediated pro-inflammatory response.**
691 (**a**) Kinome screen for a single dose of TMA (0.1 mM) against 456 kinases. (**b**) Confirmation
692 of a physical interaction between TMA and IRAK-4 using TMA at concentrations ranging
693 from 0.1 nM to 100 µM, resulting in a dissociation constant (K_d) of 14 nM. (**c**) Functional
694 characterization of the inhibition of IRAK-4 by TMA. IRAK-4 phosphorylation activity was
695 determined in presence of various concentration of TMA and resulted in an IC_{50} of 3.4 µM.
696 (**d**) Preferred binding sites of TMA from molecular dynamic simulations of IRAK-4 in
697 presence of 1% TMA. Blue grid points indicate regions with highest TMA occupancy, thereby
698 identifying several small cavities and the ATP pocket as potential binding sites. (**e-f**)
699 Assessment of the effect of 100 µM of TMA treatment on KUP5 Kupffer cells activated with
700 0.5 mM of palmitate. (**e-f**) IL6 and TNFα secretion in cell medium (n=10 biological
701 replicates). The kinases covered by the kinome scan assay are visualised using a

702 phylogenetic layout. Preliminary positive hits with potential binding >35 % vs control
703 (DMSO) are represented by a red dot whilst non-binding kinases are represented by a green
704 dot. Kinase group names: TK, Tyrosine Kinases; TKL, Tyrosine Kinase-like; STE, STE kinase
705 group; CK1, Cell Kinase 1; AGC, Protein kinase A, G and C families; CAMK, Calcium and
706 Calmodulin-regulated kinases; CMGC, CMGC kinase group. Data are means ± s.e.m. One-
707 way analysis of variance followed by Tukey's *post hoc* tests (superscript letters for factor
708 levels $P<0.05$) on log-transformed data.
709
710 **Figure 5. IRAK-4 deficiency corrects IGT and pro-inflammatory response after 8 weeks of**
711 **low choline HFD feeding in C57BL/6 mice and a chemical inhibitor of IRAK-4 mimics the**
712 **effects on glucose homeostasis.** (**a-g**) 5-week-old *Irak4*$^{-/-}$ mice and WT littermates were fed
713 a low-choline HFD (10 WT HFD and 8 *Irak4*$^{-/-}$ HFD) and were phenotyped after 8 weeks. (**a**)
714 Plasma glucose concentration during an ipGTT. (**b**) Area under the curve of the plasma
715 glucose concentration during an ipGTT. (**c-e**) Circulating cytokines (**c**) IL6, (**d**) TNFα, (**e**) IL1β.
716 (**f-h**) Liver mRNA expressions for *Saa1* (**f**), *Saa2* (**g**) and *Saa3* (**h**) genes. (**i-n**) Mice were
717 weaned at 3 weeks and fed a low-choline HFD before being fitted with osmotic minipumps
718 delivering a chronic circulating dose of PF06650833 (50 nM) for 6 weeks. (**i**) Plasma glucose
719 concentration during an ipGTT. (**j**) Area under the curve of the plasma glucose concentration
720 during an ipGTT. (**k**) Plasma glucose concentration during an ipITT. (**l**) Area under the curve
721 of the plasma glucose concentration during an ipITT. (**m-n**) Western-blot analysis of liver Akt
722 phosphorylation. Data are means ± s.e.m. Student's T-test ($P<0.05$) on log-transformed
723 data.
724
725 **Fig. 6. Overview of effects of IRAK-4 inhibition by TMA on metabolic response to HFD.**
726 TMA, which is synthesized from dietary choline (1) by the gut microbiota (2) specifically
727 inhibits IRAK-4 activity (3). This inhibition blunts the TLR signalling pathway (induced by LPS
728 and saturated free fatty acids) leading to an improvement of metabolic response to HFD
729 (e.g. glucose homeostasis).
730
731

732 **Supplementary Figure Legends**

733

734 **Supplementary Figure 1. C57BL/6 mice fed HFD display low acute-phase gene expression**
735 **in liver paralleled by high TMA excretion.** Male mice were weaned at 3 weeks and fed a
736 CHD diet, before being randomly assigned to CHD group (n=270) or HFD (n=202) groups and
737 monitored at 2 (72 CHD and 64 HFD), 3 (84 CHD and 57 HFD), 5 (68 CHD and 47 HFD) and 7
738 months (46 CHD and 34 HFD). (**a-c**) Effect of HFD-feeding on physiological parameters. (**a**)
739 Body weight (BW), (**b**) glucose tolerance test (GTT) at 5 months and (**c**) cumulative glycemia
740 during GTT (AUC). (**d-e**) Effect of HFD-feeding on liver transcriptome at 5 months. (**d**)
741 Volcano plot of differentially expressed genes, highlighting that *Saa1* and *Saa2* are down-
742 regulated in HFD. Red dots, significantly (FDR < 0.1) differentially expressed genes. (**e**)
743 Heatmap of significantly (FDR < 0.1) differentially expressed genes. (**f-i**) Effect of HFD-
744 feeding and age on urinary metabolic phenotypes analyzed by ^{1}H-NMR spectroscopy. (**f**) ^{1}H-
745 NMR-based metabotyping scores plot from a cross-validated O-PLS-DA model segregating
746 the eight groups of mice according to both diet and age. (**g**) Empirical assessment of the
747 significance of O-PLS goodness-of-fit parameters by generating a null distribution with
748 10,000 random permutations. (**h**) Metabolic signature of diet on O-PLS model coefficient
749 plot; line plot corresponds to covariance and the color-scale represents proportion of
750 variance explained. (**i**) Assessment of the contribution of factors diet and age on choline,
751 TMA and TMAO by O-PLS variance components analysis. Data are means ± s.e.m. Two-sided
752 Mann-Whitney test (*P < 0.05 vs control). For the O-PLS-DA permutation test, the horizontal
753 axis corresponds to the correlation between the original class membership variable (single
754 dots on the right) and the randomly permuted class membership vectors (no longer
755 correlated with the original class membership) (swarm of permutated models on the left).
756 The y axis corresponds to goodness-of-fit parameter R^2 (in green) derived for each O-PLS-DA
757 model and the goodness-of-prediction parameter Q^2 (in blue) derived by 7-fold cross-
758 validation of each O-PLS-DA model. The R^2 and Q^2 parameters obtained from the original
759 model in the top right corner are outside the confidence interval of the 10,000 randomly
760 permuted models and therefore confirming the significance of the fitness and prediction
761 capacity of the original O-PLS-DA model.

762

763 **Supplementary Fig. 2. Pathway analysis for hepatic significant genes.** (**a**) Gene ontology
764 analysis for down- and up-regulated HFD-responsive genes, (**b**) Signaling pathway impact
765 analysis for HFD-responsive genes. Pathways respectively on the right-hand side of the red
766 and blue curves are significant after Bonferroni correction of the global p-values (pG)
767 obtained by combining the pPERT and pNDE using the normal inversion method, and
768 significant after a FDR correction of pG. Significant KEGG pathways: 04141, Protein
769 processing in the endoplasmic reticulum; 04710, Circadian rhythm; 04152, AMPK signaling
770 pathway.
771
772 **Supplementary Fig. 3. Choline supplementation corrects HFD adverse effects and**
773 **associated methylamine measurements.** (**a**) Food intake measured on the three tested
774 diets (CHD, LC-HFD and HC-HFD). (**b-c**) Western blot analysis of liver NF-kB phosphotylation
775 state between LC-HFD and HC-HFD. (**d**) Plasma sample chromatogram for the simultaneous
776 detection of TMA, TMAO, choline, γ-butyrobetaine, carnitine, betaine and their isotopically
777 labelled analogues. (**e**) Principal Component Analysis Biplot of plasma methylamine
778 quantifications by UPLC/MS-MS from mice fed CHD, LC-HFD and HC-HFD. Data are means ±
779 s.e.m. Two-sided Mann-Whitney test (*P < 0.05 vs control).
780
781 **Supplementary Fig. 4. Modulation of TMa production and effects.** (**a-d**) Confirmation of
782 blockage of production of TMA (**a**, **c**) and TMAO (**b**, **d**) by 1% DMB measured in plasma (**a-b**)
783 and urine (**c-d**). (**e**) Body weight monitoring during the whole experiment of mice fed a LC-
784 HFD and a HC-HFD supplemented or not with DMB or treated with antibiotics. (**f**) Plasma
785 insulin concentration during GTT at 0, 30 and 120 min post glucose injection. (**g**) Body
786 weight monitoring during the whole experiment of mice fed a LC-HFD and chronically
787 treated with TMA. (**h**) Plasma insulin concentration during GTT at 0, 30 and 120 min post
788 glucose injection. Data are means ± s.e.m. Two-sided Mann-Whitney test (*P < 0.05 vs LC-
789 HFD control).
790
791 **Supplementary Fig. 5. TMA does not bind with kinases ANKK1, HIPK2, JAK2, and NDR1**
792 **identified as candidates in the kinome screen, but makes significant contact with IRAK-4.**
793 (**a-d**) Physical interaction test between TMA and the four hits identified using a kinome
794 screen, using TMA concentrations ranging from 0.1 nM to 100 μM for (**a**) ANKK1, (**b**) HIPK2,

795 (**c**) JAK2 and (**d**) NDR1. (**e-g**) IRAK-4 activity is not inhibited by choline (**e**), TMAO (**f**) or DMB
796 (**g**), while TMA does not have any inhibitory effect on IRAK-1 (**h**). (**i-j**) Molecular dynamic
797 parameters and outputs (**i**) force-field parameters and (**j**) number of protein-ligand H bonds
798 and contacts with 1% of TMA. (**k**) Optimisation of palmitate dose on IL6 secretion by KUP5
799 cells. Data are means ± s.e.m. One-way ANOVA followed by Tukey's *post hoc* tests
800 (superscript letters for factor levels $P<0.05$) on log-transformed data.
801
802 **Supplementary Fig. 6. IRAK-4 knock-out does not affect body weight while chronic**
803 **treatment with PF06650833 reduces it in mice fed a low-choline HFD.** (**a-b**) Body weight
804 monitoring during the whole experiment of *Irak4*$^{-/-}$ mice (**a**) or PF06650833-treated mice (**b**)
805 fed a LC-HFD.
806
807 **Supplementary Tab. 1: Hepatic genes differentially expressed by HFD-feeding.** Hepatic
808 transcriptomes were analysed using Limma[54] and genes are considered significant if Fdr<0.1.
809
810 **Supplementary Tab. 2: Down-regulated HFD-responsive hepatic pathways.** Gene ontology
811 analysis was performed using Enrichr[55] and pathways are considered significant if Fdr<0.1.
812
813 **Supplementary Tab. 3: Up-regulated HFD-responsive hepatic genes.** Gene ontology
814 analysis was performed using Enrichr[55] and pathways are considered significant if Fdr<0.1.
815
816 **Supplementary Tab. 4: Hepatic signalling pathways impacted by HFD.** Signalling pathway
817 impact analysis was performed using SPIA[56] and pathways are considered significant if
818 pGFWER<0.1.
819
820 **Supplementary Tab. 5. TMA kinome screen.** Screening results for single-dose TMA binding
821 to 456 kinases. "Percent control" corresponds to the percentage of DNA amplified by qPCR
822 compared to the control condition. Values below 35 % (in green) are considered as positive
823 hits.
824

825 **Supplementary Tab. 6. Diet formulations.** Sepcific fat, protein, carbohydrate and choline
826 content in regimens formulated by Research Diet are summarized based on %w/w and
827 %kcal.

828 **Online References.**
829

830 50. Fearnside, J. F. *et al.* Phylometabonomic patterns of adaptation to high fat diet
831 feeding in inbred mice. *PLoS ONE* **3,** e1668 (2008).
832 51. Geurts, L., Muccioli, G. G., Delzenne, N. M. & Cani, P. D. Chronic endocannabinoid
833 system stimulation induces muscle macrophage and lipid accumulation in type 2
834 diabetic mice independently of metabolic endotoxaemia. *PLoS ONE* **8,** e55963 (2013).
835 52. Toye, A. A. *et al.* Subtle metabolic and liver gene transcriptional changes underlie
836 diet-induced fatty liver susceptibility in insulin-resistant mice. *Diabetologia* **50,** 1867–
837 1879 (2007).
838 53. Gentleman, R., Carey, V. J., Huber, W., Irizarry, R. A. & Dudoit, S. *Bioinformatics and*
839 *Computational Biology Solutions Using R and Bioconductor*. (Springer, 2006).
840 54. Smyth, G. K. in *… and computational biology solutions using R and …* 397–420
841 (Springer-Verlag, 2005). doi:10.1007/0-387-29362-0_23
842 55. Chen, E. Y. *et al.* Enrichr: interactive and collaborative HTML5 gene list enrichment
843 analysis tool. *BMC Bioinformatics* **14,** 128 (2013).
844 56. Tarca, A. L. *et al.* A novel signaling pathway impact analysis. *Bioinformatics* **25,** 75–82
845 (2009).
846 57. Blaise, B. J. *et al.* Metabotyping of Caenorhabditis elegans reveals latent phenotypes.
847 *Proc. Natl. Acad. Sci. U.S.A.* **104,** 19808–19812 (2007).
848 58. Salomon-Ferrer, R., Götz, A. W., Poole, D., Le Grand, S. & Walker, R. C. Routine
849 Microsecond Molecular Dynamics Simulations with AMBER on GPUs. 2. Explicit
850 Solvent Particle Mesh Ewald. *J. Chem. Theory Comput.* **9,** 3878−3888 (2013).
851 59. Wang, Z. *et al.* Crystal structures of IRAK-4 kinase in complex with inhibitors: a
852 serine/threonine kinase with tyrosine as a gatekeeper. *Structure* **14,** 1835–1844
853 (2006).
854 60. Labute, P. Protonate3D: assignment of ionization states and hydrogen coordinates to
855 macromolecular structures. *Proteins* **75,** 187–205 (2009).
856 61. Lindorff-Larsen, K. *et al.* Improved side-chain torsion potentials for the Amber ff99SB
857 protein force field. *Proteins* **78,** 1950–1958 (2010).
858 62. Wang, J., Wolf, R. M., Caldwell, J. W., Kollman, P. A. & Case, D. A. Development and
859 testing of a general amber force field. *J Comput Chem* **25,** 1157–1174 (2004).
860 63. Jorgensen, W. L., Chandrasekhar, J., Madura, J. D., Impey, R. W. & Klein, M. L.
861 Comparison of simple potential functions for simulating liquid water. *J. Chem. Phys.*
862 **79,** 926–935 (1983).
863 64. Fuchs, J. E. *et al.* Dynamic regulation of phenylalanine hydroxylase by simulated redox
864 manipulation. *PLoS ONE* **7,** e53005 (2012).
865 65. Roe, D. R. & Cheatham, T. E., III. PTRAJ and CPPTRAJ: Software for Processing and
866 Analysis of Molecular Dynamics Trajectory Data. *J. Chem. Theory Comput.* **9,** 3084–
867 3095 (2013).
868 66. Kuglstatter, A. *et al.* Cutting Edge: IL-1 receptor-associated kinase 4 structures reveal
869 novel features and multiple conformations. *J. Immunol.* **178,** 2641–2645 (2007).

870

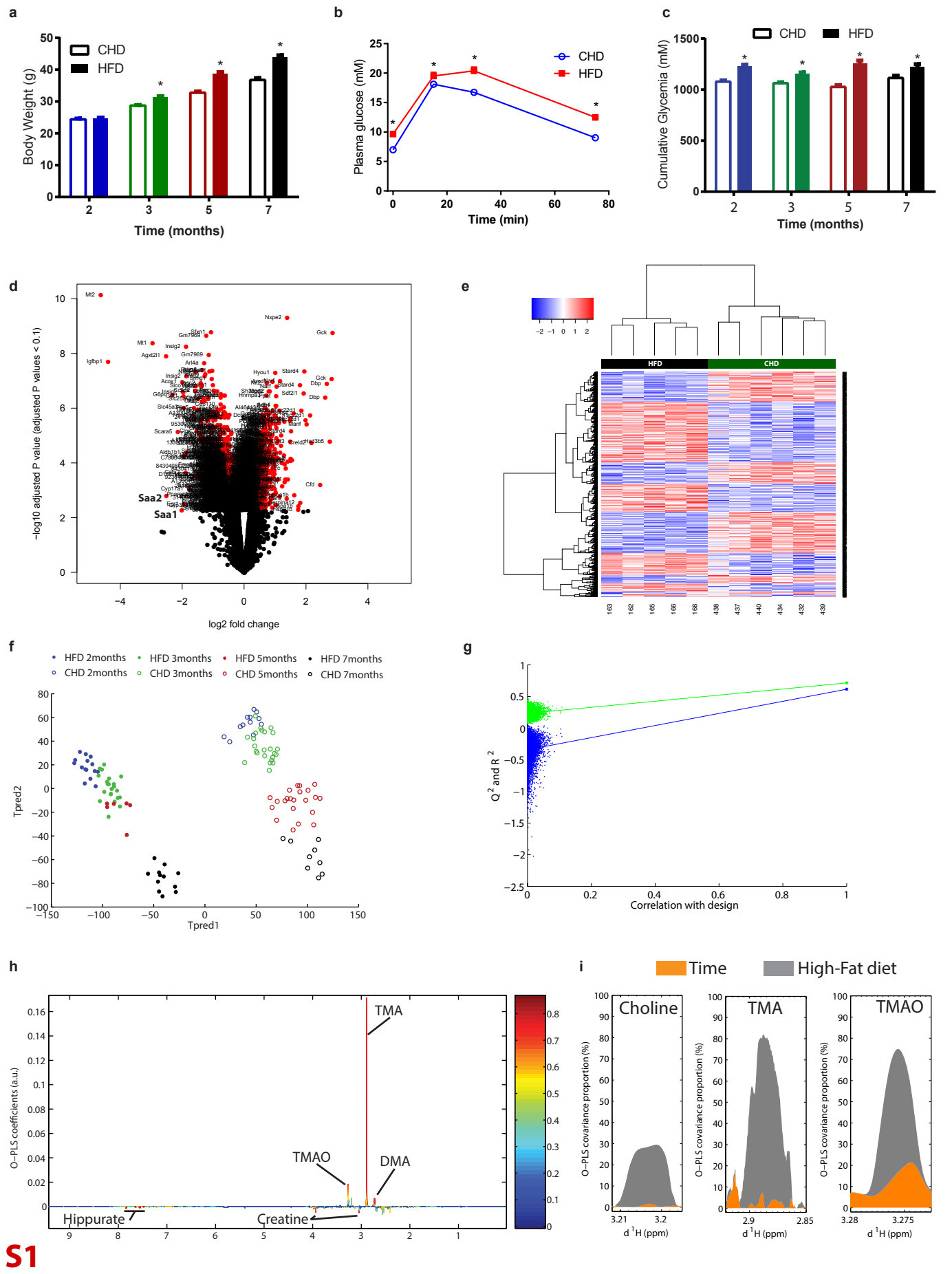
a
Body Weight (g)
CHD
HFD
Time (months)
b
Plasma glucose (mM)
CHD
HFD
Time (min)
c
Cumulative Glycemia (mM)
CHD
HFD
Time (months)
d
−log10 adjusted P value (adjusted P values < 0.1)
log2 fold change
Saa2
Saa1
e
HFD
CHD
f
HFD 2months
HFD 3months
HFD 5months
HFD 7months
CHD 2months
CHD 3months
CHD 5months
CHD 7months
Tpred1
Tpred2
g
Correlation with design
h
O−PLS coefficients (a.u.)
TMA
TMAO
DMA
Hippurate
Creatine
i
Time
High-Fat diet
Choline
TMA
TMAO
O−PLS covariance proportion (%)
d 1H (ppm)

S1

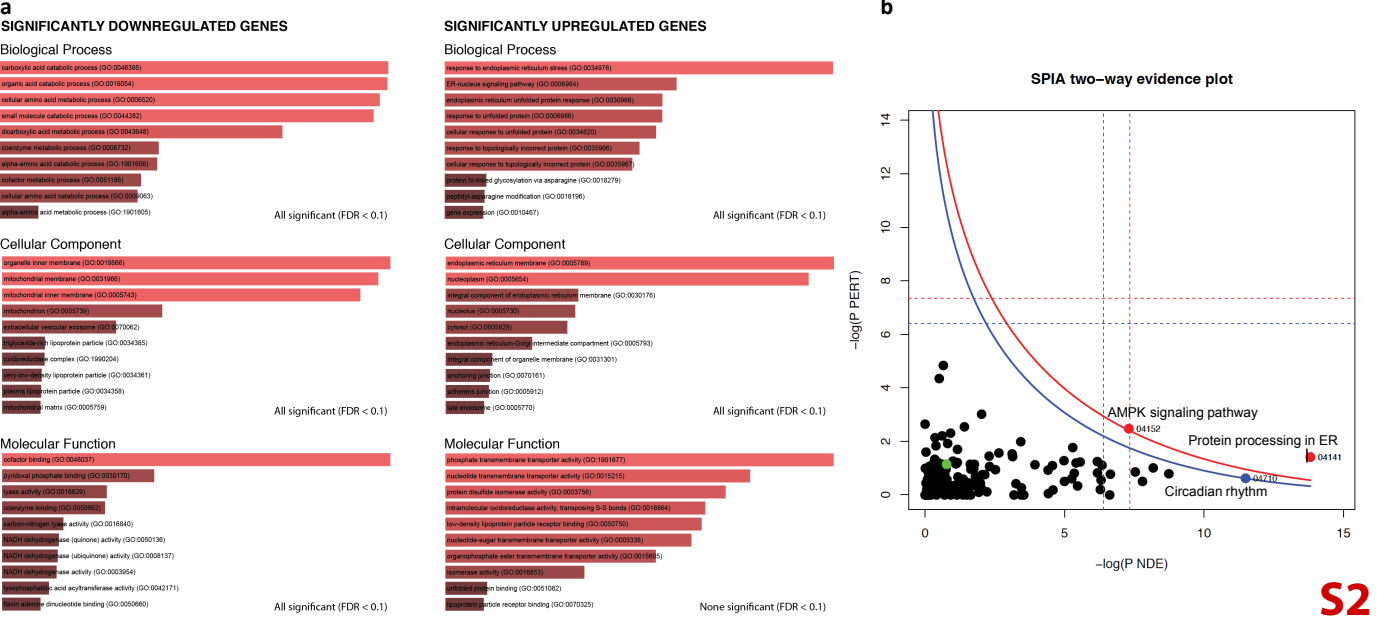
a
SIGNIFICANTLY DOWNREGULATED GENES
Biological Process
carboxylic acid catabolic process (GO:0046395)
organic acid catabolic process (GO:0016054)
cellular amino acid metabolic process (GO:0006520)
small molecule catabolic process (GO:0044282)
dicarboxylic acid metabolic process (GO:0043648)
coenzyme metabolic process (GO:0006732)
alpha-amino acid catabolic process (GO:1901606)
cofactor metabolic process (GO:0051186)
cellular amino acid catabolic process (GO:0009063)
alpha-amino acid metabolic process (GO:1901605)
All significant (FDR < 0.1)
Cellular Component
organelle inner membrane (GO:0019866)
mitochondrial membrane (GO:0031966)
mitochondrial inner membrane (GO:0005743)
mitochondrion (GO:0005739)
extracellular vesicular exosome (GO:0070062)
triglyceride-rich lipoprotein particle (GO:0034385)
oxidoreductase complex (GO:1990204)
very-low-density lipoprotein particle (GO:0034361)
plasma lipoprotein particle (GO:0034358)
mitochondrial matrix (GO:0005759)
All significant (FDR < 0.1)
Molecular Function
cofactor binding (GO:0048037)
pyridoxal phosphate binding (GO:0030170)
lyase activity (GO:0016829)
coenzyme binding (GO:0050662)
carbon-nitrogen lyase activity (GO:0016840)
NADH dehydrogenase (quinone) activity (GO:0050136)
NADH dehydrogenase (ubiquinone) activity (GO:0008137)
NADH dehydrogenase activity (GO:0003954)
lysophosphatidic acid acyltransferase activity (GO:0042171)
flavin adenine dinucleotide binding (GO:0050660)
All significant (FDR < 0.1)
SIGNIFICANTLY UPREGULATED GENES
Biological Process
response to endoplasmic reticulum stress (GO:0034976)
ER-nucleus signaling pathway (GO:0006984)
endoplasmic reticulum unfolded protein response (GO:0030968)
response to unfolded protein (GO:0006986)
cellular response to unfolded protein (GO:0034620)
response to topologically incorrect protein (GO:0035966)
cellular response to topologically incorrect protein (GO:0035967)
protein N-linked glycosylation via asparagine (GO:0018279)
peptidyl-asparagine modification (GO:0018196)
gene expression (GO:0010467)
All significant (FDR < 0.1)
Cellular Component
endoplasmic reticulum membrane (GO:0005789)
nucleoplasm (GO:0005654)
integral component of endoplasmic reticulum membrane (GO:0030176)
nucleolus (GO:0005730)
cytosol (GO:0005829)
endoplasmic reticulum-Golgi intermediate compartment (GO:0005793)
integral component of organelle membrane (GO:0031301)
anchoring junction (GO:0070161)
adherens junction (GO:0005912)
late endosome (GO:0005770)
All significant (FDR < 0.1)
Molecular Function
phosphate transmembrane transporter activity (GO:1901677)
nucleotide transmembrane transporter activity (GO:0015215)
protein disulfide isomerase activity (GO:0003756)
intramolecular oxidoreductase activity, transposing S-S bonds (GO:0016864)
low-density lipoprotein particle receptor binding (GO:0050750)
nucleotide-sugar transmembrane transporter activity (GO:0005338)
organophosphate ester transmembrane transporter activity (GO:0015605)
isomerase activity (GO:0016853)
unfolded protein binding (GO:0051082)
lipoprotein particle receptor binding (GO:0070325)
None significant (FDR < 0.1)
b
SPIA two−way evidence plot
−log(P PERT)
−log(P NDE)
0
2
4
6
8
10
12
14
0
5
10
15
AMPK signaling pathway
04152
Protein processing in ER
04141
04710
Circadian rhythm
S2

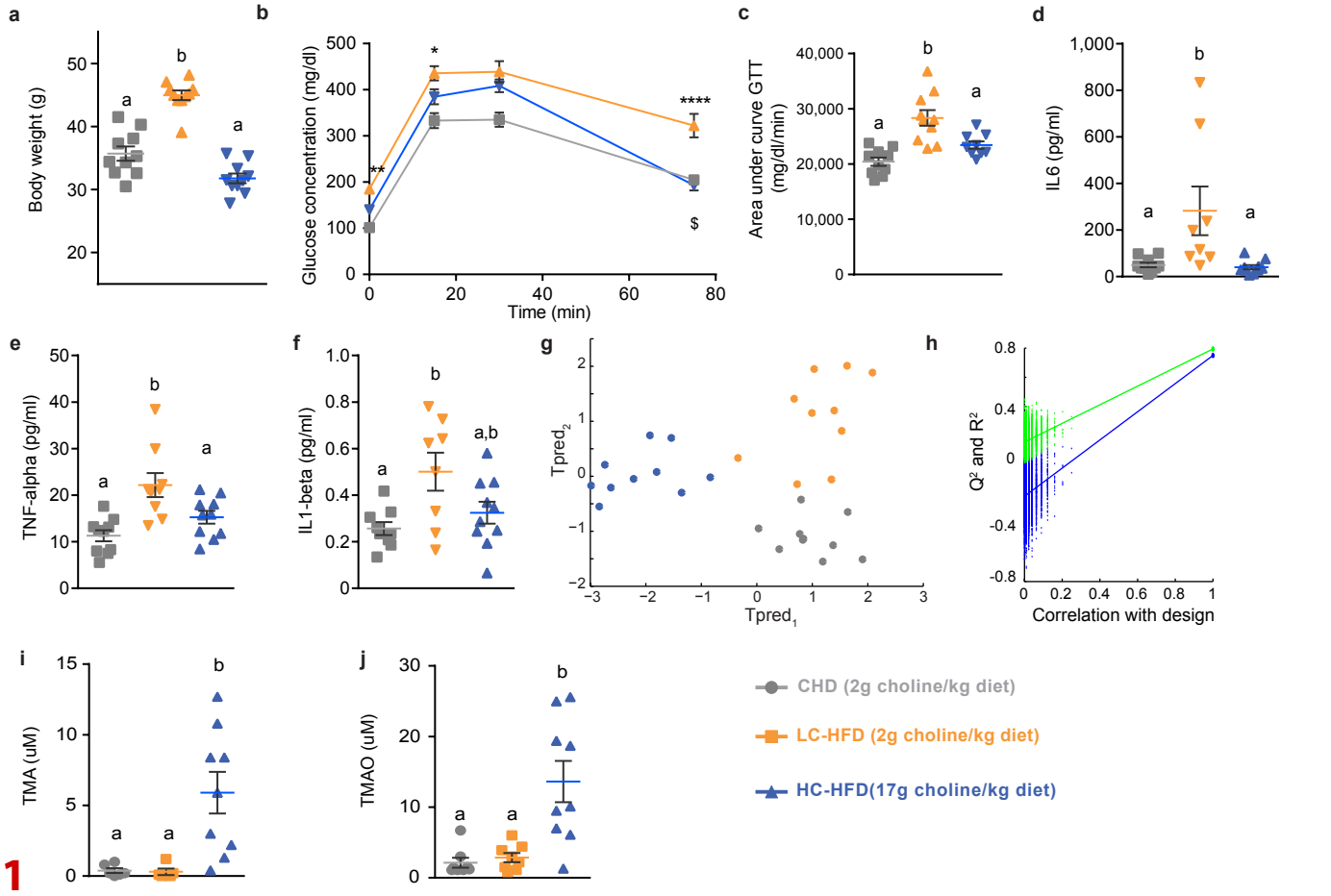
a
Body weight (g)
b
Glucose concentration (mg/dl)
Time (min)
c
Area under curve GTT (mg/dl/min)
d
IL6 (pg/ml)
e
TNF-alpha (pg/ml)
f
IL1-beta (pg/ml)
g
Tpred2
Tpred1
h
Q2 and R2
Correlation with design
i
TMA (uM)
j
TMAO (uM)
CHD (2g choline/kg diet)
LC-HFD (2g choline/kg diet)
HC-HFD(17g choline/kg diet)

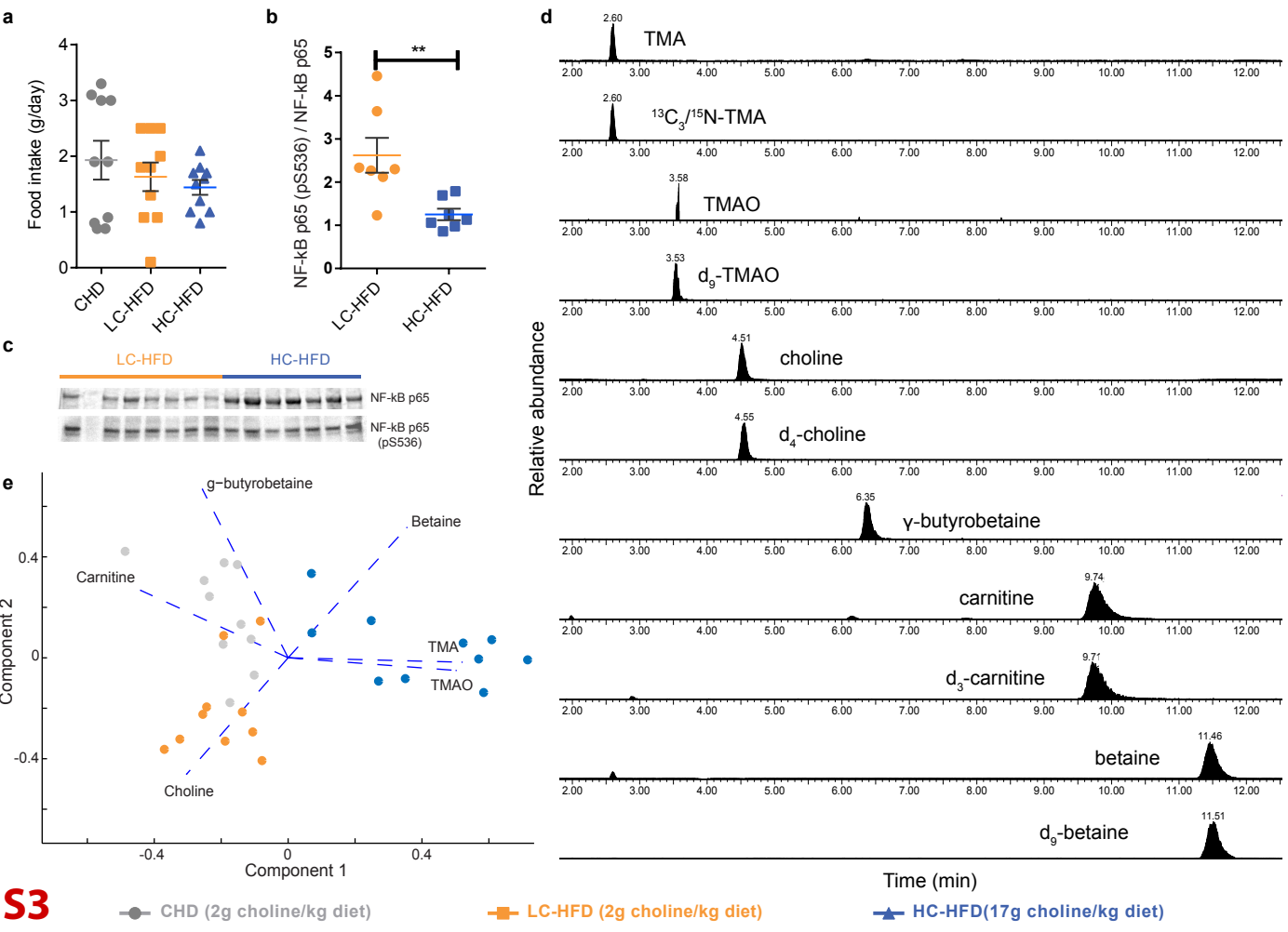
a
Food intake (g/day)
CHD
LC-HFD
HC-HFD
b
NF-kB p65 (pS536) / NF-kB p65
**
LC-HFD
HC-HFD
c
LC-HFD
HC-HFD
NF-kB p65
NF-kB p65 (pS536)
d
TMA
13C3/15N-TMA
TMAO
d9-TMAO
choline
d4-choline
γ-butyrobetaine
carnitine
d3-carnitine
betaine
d9-betaine
Relative abundance
Time (min)
e
g-butyrobetaine
Betaine
Carnitine
TMA
TMAO
Choline
Component 1
Component 2
S3
CHD (2g choline/kg diet)
LC-HFD (2g choline/kg diet)
HC-HFD(17g choline/kg diet)

CHD (2g choline/kg diet) LC-HFD (2g choline/kg diet) HC-HFD(17g choline/kg diet)

a

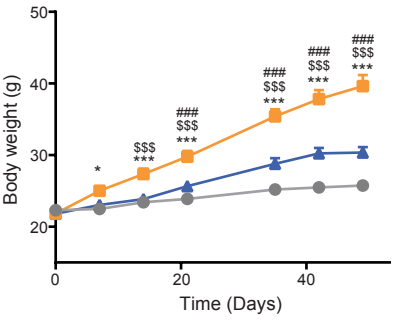

b

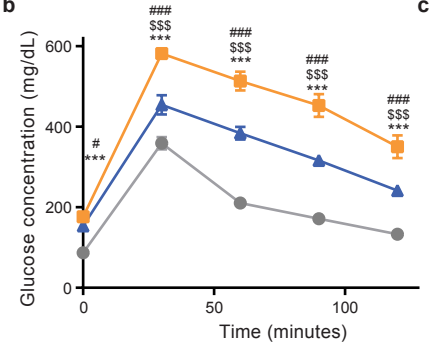

c

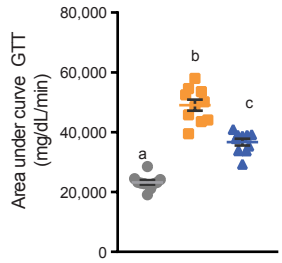

d

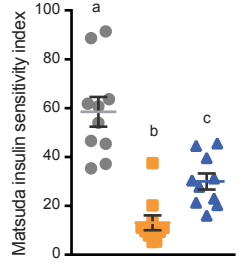

e

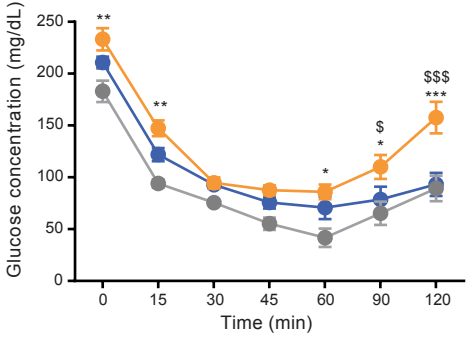

f

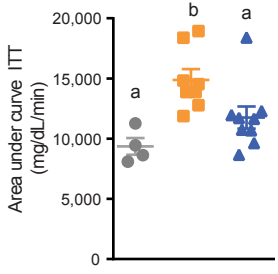

g

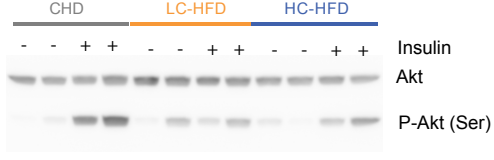

i

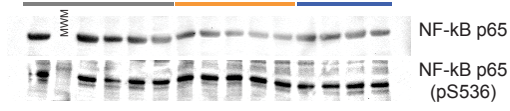

h

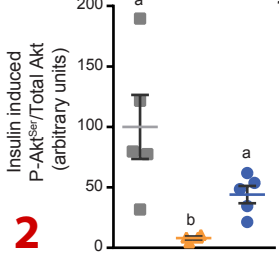

j

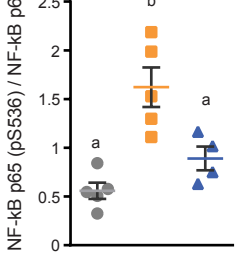

k

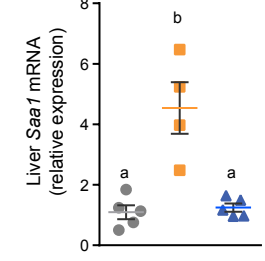

l

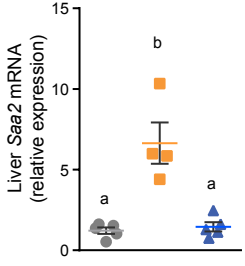

m

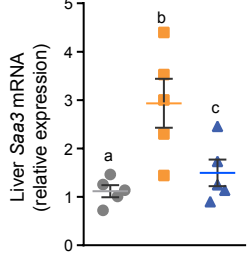

2

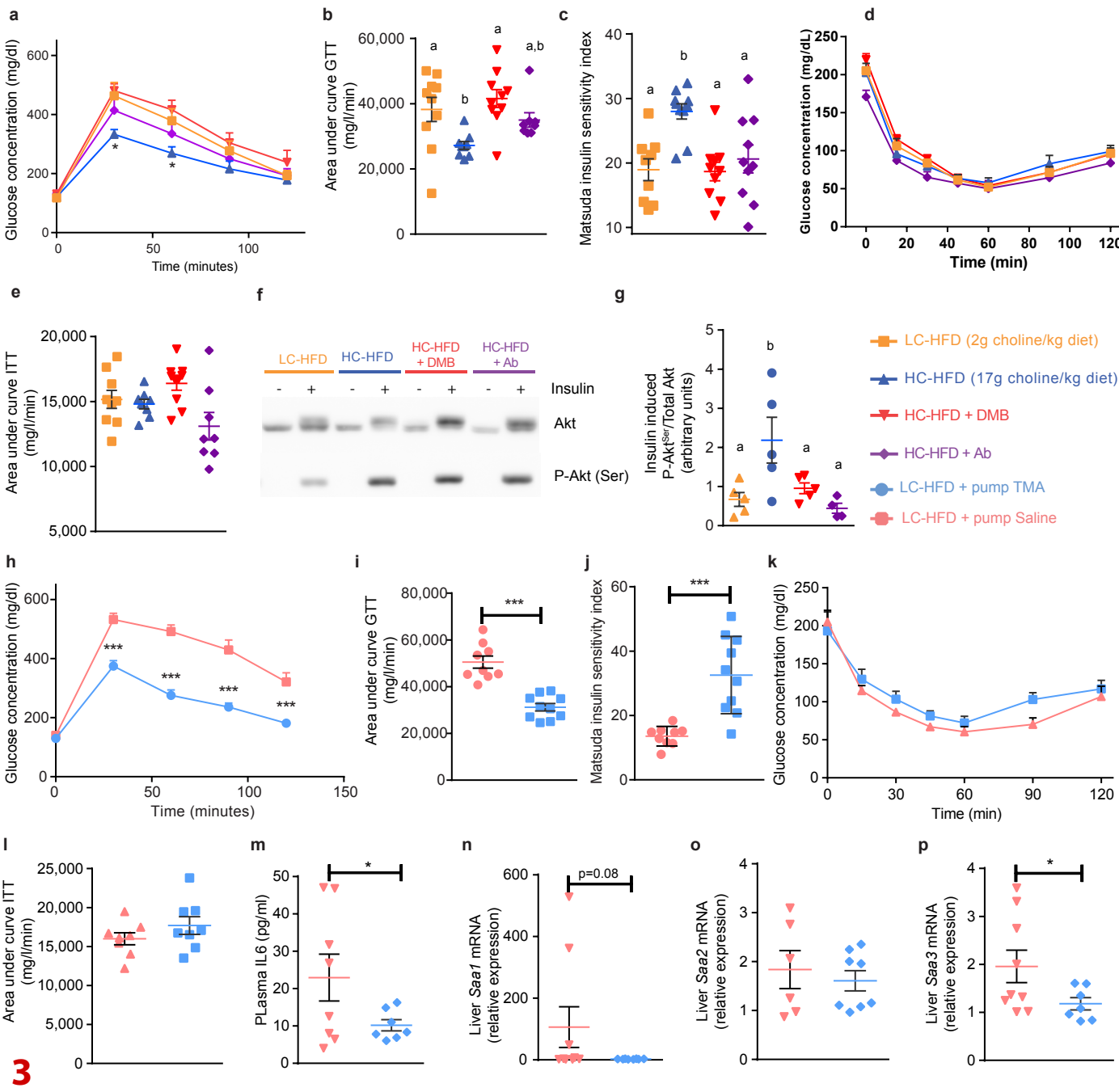
a
Glucose concentration (mg/dl)
Time (minutes)
b
Area under curve GTT (mg/l/min)
c
Matsuda insulin sensitivity index
d
Glucose concentration (mg/dL)
Time (min)
e
Area under curve ITT (mg/l/min)
f
LC-HFD
HC-HFD
HC-HFD + DMB
HC-HFD + Ab
Insulin
Akt
P-Akt (Ser)
g
Insulin induced P-Akt^Ser/Total Akt (arbitrary units)
LC-HFD (2g choline/kg diet)
HC-HFD (17g choline/kg diet)
HC-HFD + DMB
HC-HFD + Ab
LC-HFD + pump TMA
LC-HFD + pump Saline
h
Glucose concentration (mg/dl)
Time (minutes)
i
Area under curve GTT (mg/l/min)
j
Matsuda insulin sensitivity index
k
Glucose concentration (mg/dl)
Time (min)
l
Area under curve ITT (mg/l/min)
m
PLasma IL6 (pg/ml)
n
Liver Saa1 mRNA (relative expression)
p=0.08
o
Liver Saa2 mRNA (relative expression)
p
Liver Saa3 mRNA (relative expression)
3

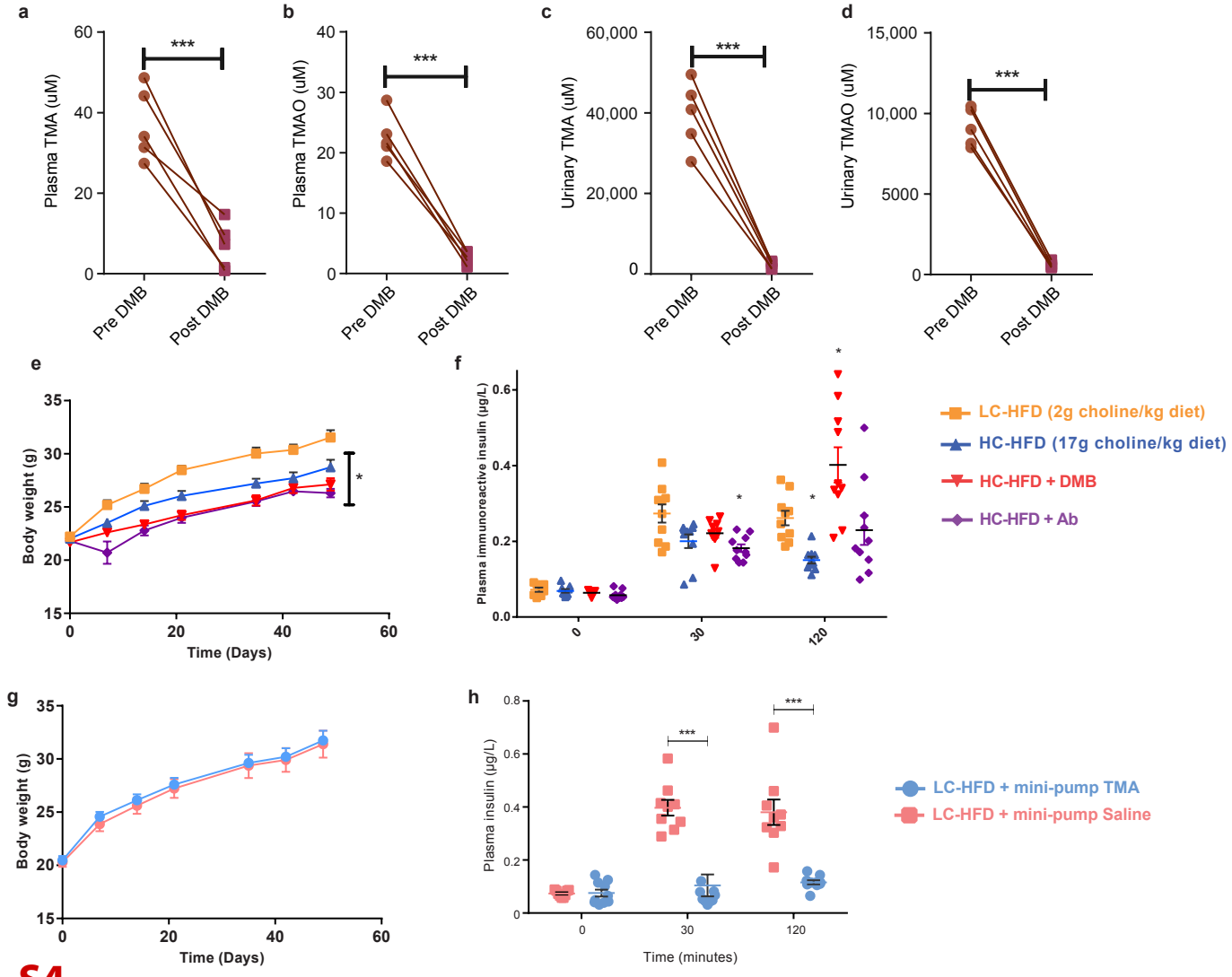
a
Plasma TMA (uM)
60
40
20
0
***
Pre DMB
Post DMB
b
Plasma TMAO (uM)
40
30
20
10
0
***
Pre DMB
Post DMB
c
Urinary TMA (uM)
60,000
40,000
20,000
0
***
Pre DMB
Post DMB
d
Urinary TMAO (uM)
15,000
10,000
5000
0
***
Pre DMB
Post DMB
e
Body weight (g)
35
30
25
20
15
0
20
40
60
Time (Days)
*
f
Plasma immunoreactive insulin (µg/L)
0.6
0.4
0.2
0.0
0
30
120
*
*
*
LC-HFD (2g choline/kg diet)
HC-HFD (17g choline/kg diet)
HC-HFD + DMB
HC-HFD + Ab
g
Body weight (g)
35
30
25
20
15
0
20
40
60
Time (Days)
h
Plasma insulin (µg/L)
0.8
0.6
0.4
0.2
0
***
***
0
30
120
Time (minutes)
LC-HFD + mini-pump TMA
LC-HFD + mini-pump Saline

S4

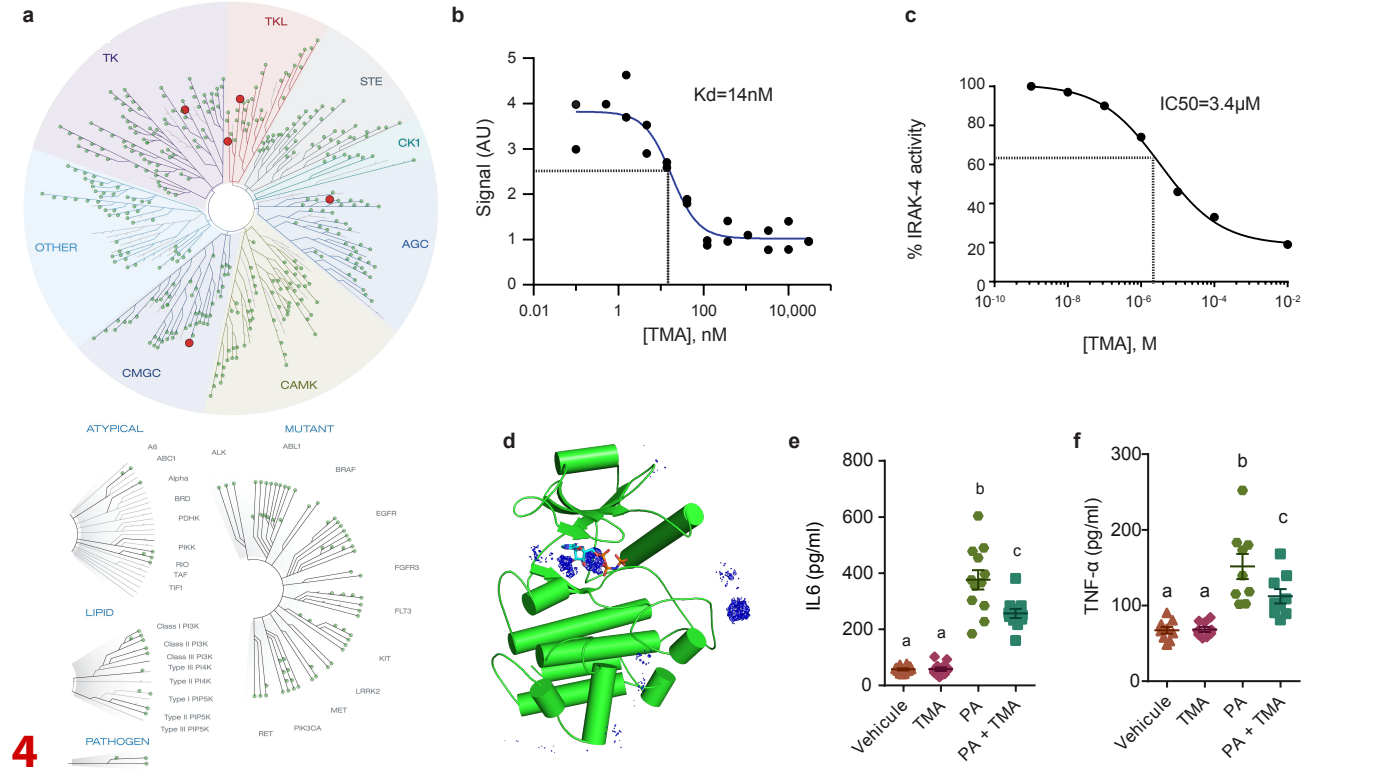
a
TKL
TK
STE
CK1
OTHER
AGC
CMGC
CAMK
ATYPICAL
A6
ABC1
Alpha
BRD
PDHK
PIKK
RIO
TAF
TIF1
MUTANT
ALK
ABL1
BRAF
EGFR
FGFR3
FLT3
KIT
LRRK2
MET
PIK3CA
RET
LIPID
Class I PI3K
Class II PI3K
Class III PI3K
Type III PI4K
Type II PI4K
Type I PIP5K
Type II PIP5K
Type III PIP5K
PATHOGEN
b
Kd=14nM
Signal (AU)
[TMA], nM
0.01
1
100
10,000
c
IC50=3.4μM
% IRAK-4 activity
[TMA], M
d
e
IL6 (pg/ml)
Vehicule
TMA
PA
PA + TMA
f
TNF-α (pg/ml)
Vehicule
TMA
PA
PA + TMA

4

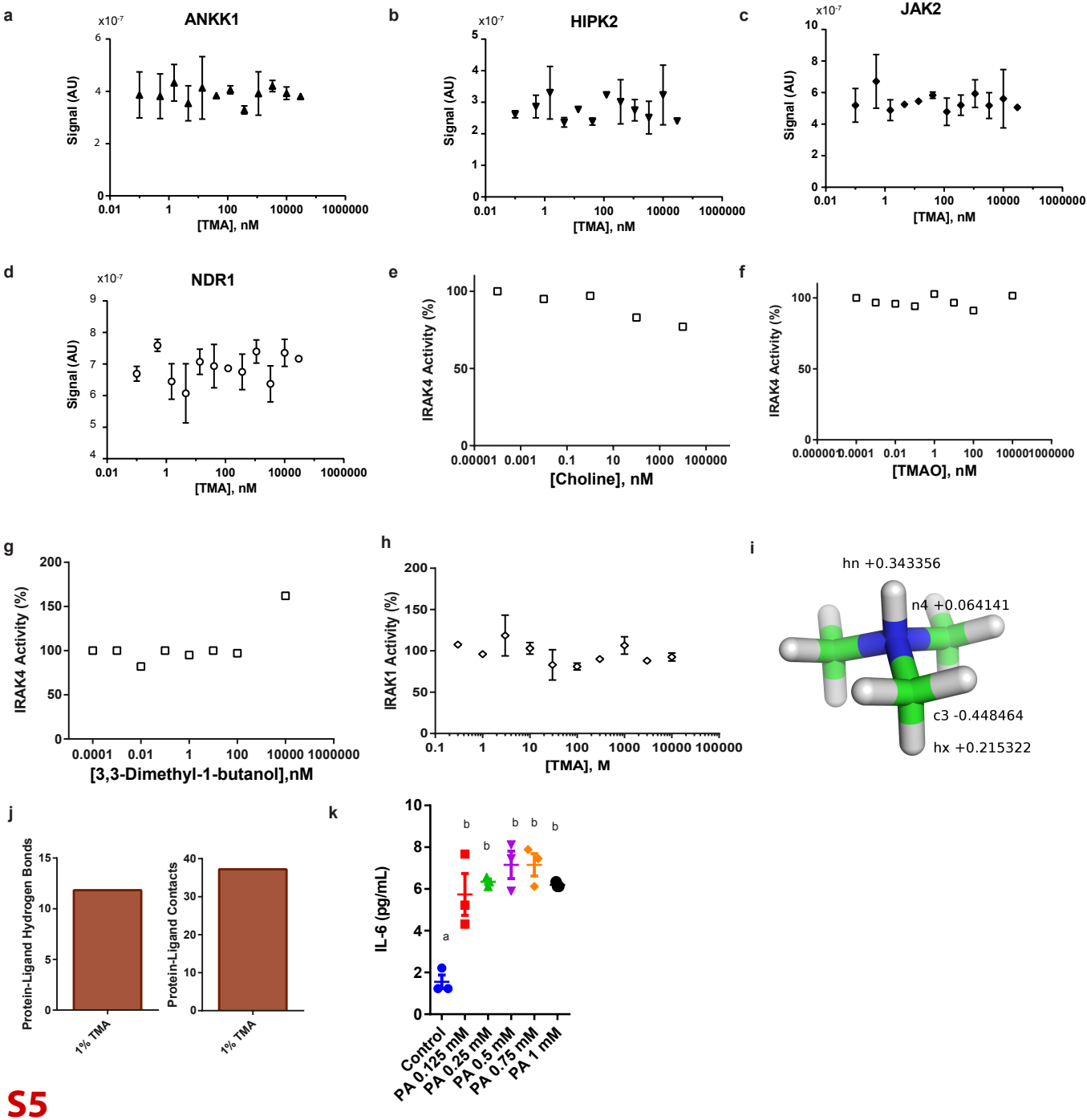
a
ANKK1
x10-7
Signal (AU)
[TMA], nM
b
HIPK2
c
JAK2
d
NDR1
e
IRAK4 Activity (%)
[Choline], nM
f
[TMAO], nM
g
[3,3-Dimethyl-1-butanol],nM
h
IRAK1 Activity (%)
[TMA], M
i
hn +0.343356
n4 +0.064141
c3 -0.448464
hx +0.215322
j
Protein-Ligand Hydrogen Bonds
Protein-Ligand Contacts
1% TMA
k
IL-6 (pg/mL)
Control
PA 0.125 mM
PA 0.25 mM
PA 0.5 mM
PA 0.75 mM
PA 1 mM

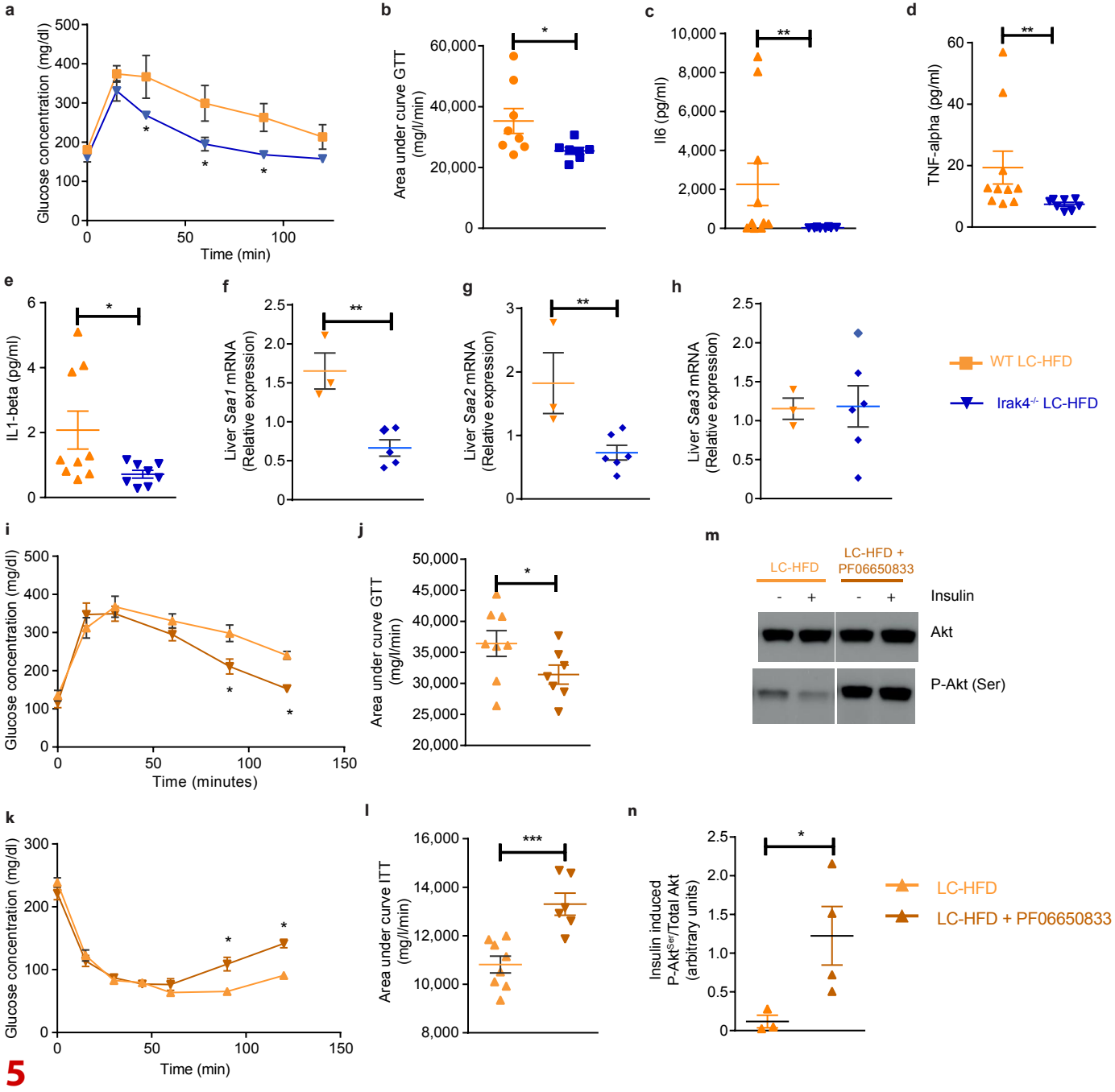
a
Glucose concentration (mg/dl)
Time (min)
b
Area under curve GTT (mg/l/min)
c
Il6 (pg/ml)
d
TNF-alpha (pg/ml)
e
IL1-beta (pg/ml)
f
Liver Saa1 mRNA (Relative expression)
g
Liver Saa2 mRNA (Relative expression)
h
Liver Saa3 mRNA (Relative expression)
WT LC-HFD
Irak4-/- LC-HFD
i
Glucose concentration (mg/dl)
Time (minutes)
j
Area under curve GTT (mg/l/min)
m
LC-HFD
LC-HFD + PF06650833
Insulin
Akt
P-Akt (Ser)
k
Glucose concentration (mg/dl)
Time (min)
l
Area under curve ITT (mg/l/min)
n
Insulin induced P-Akt^Ser/Total Akt (arbitrary units)
LC-HFD
LC-HFD + PF06650833

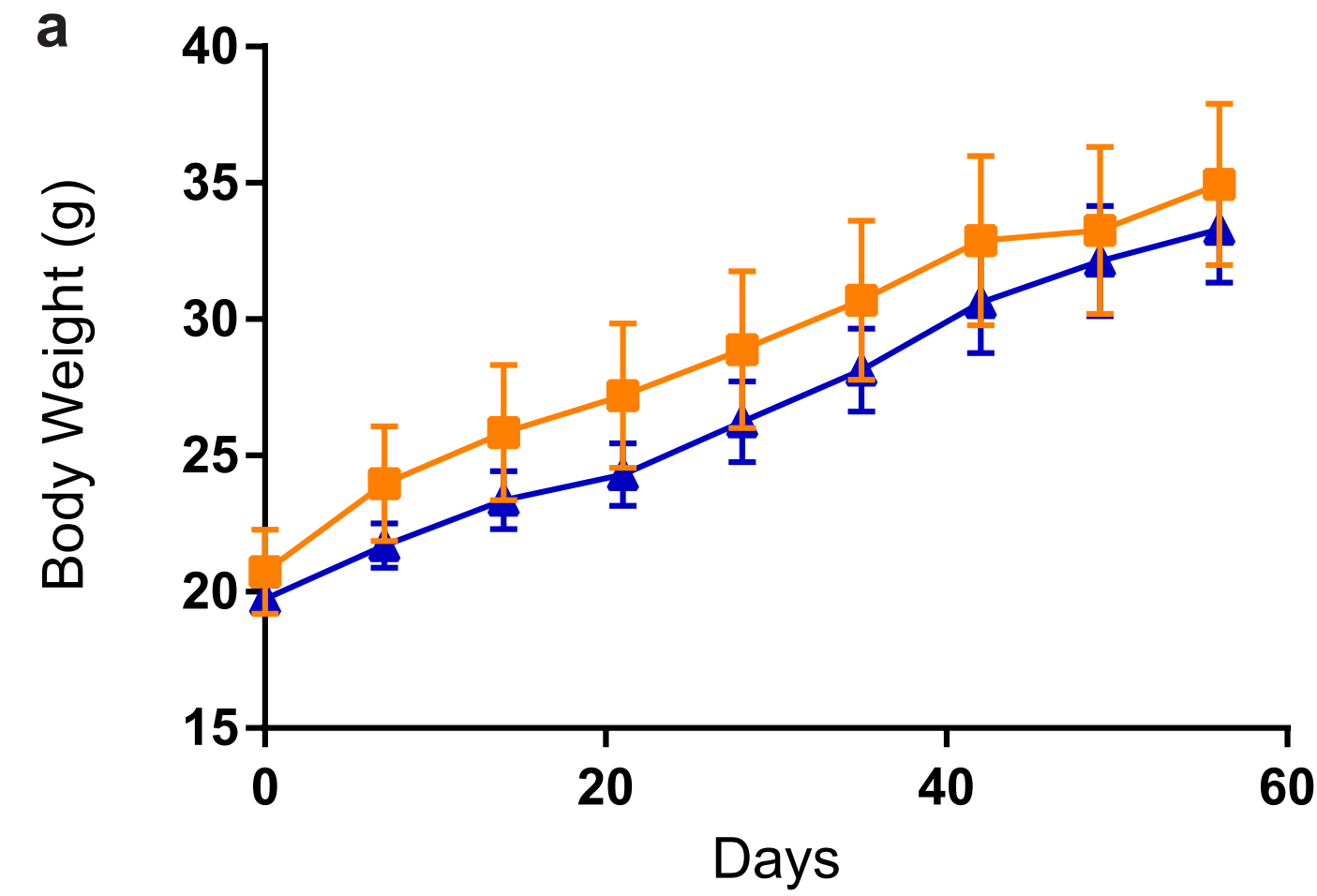
a
Body Weight (g)
40
35
30
25
20
15
0
20
40
60
Days

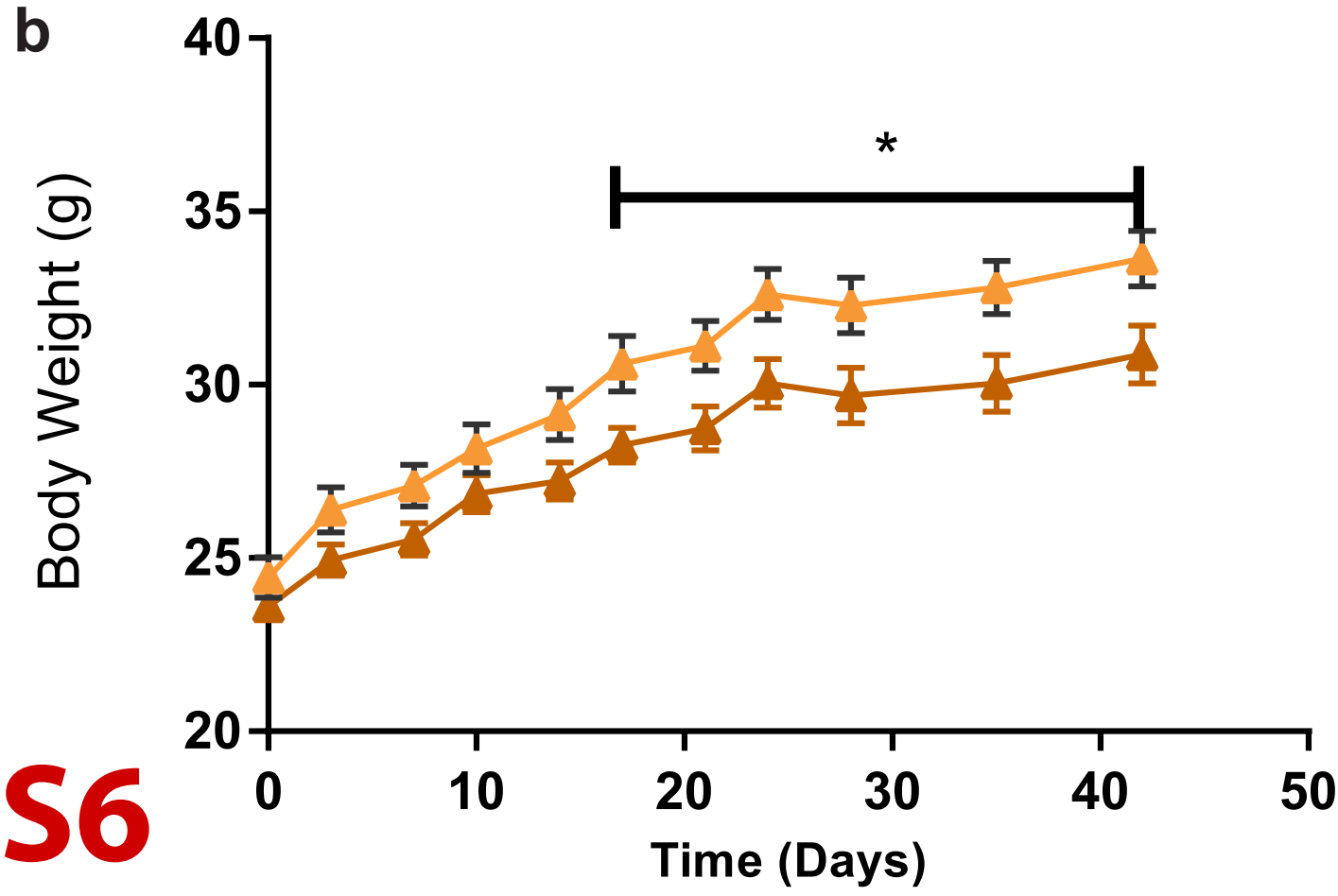
b
Body Weight (g)
40
35
30
25
20
*
0
10
20
30
40
50
Time (Days)

S6

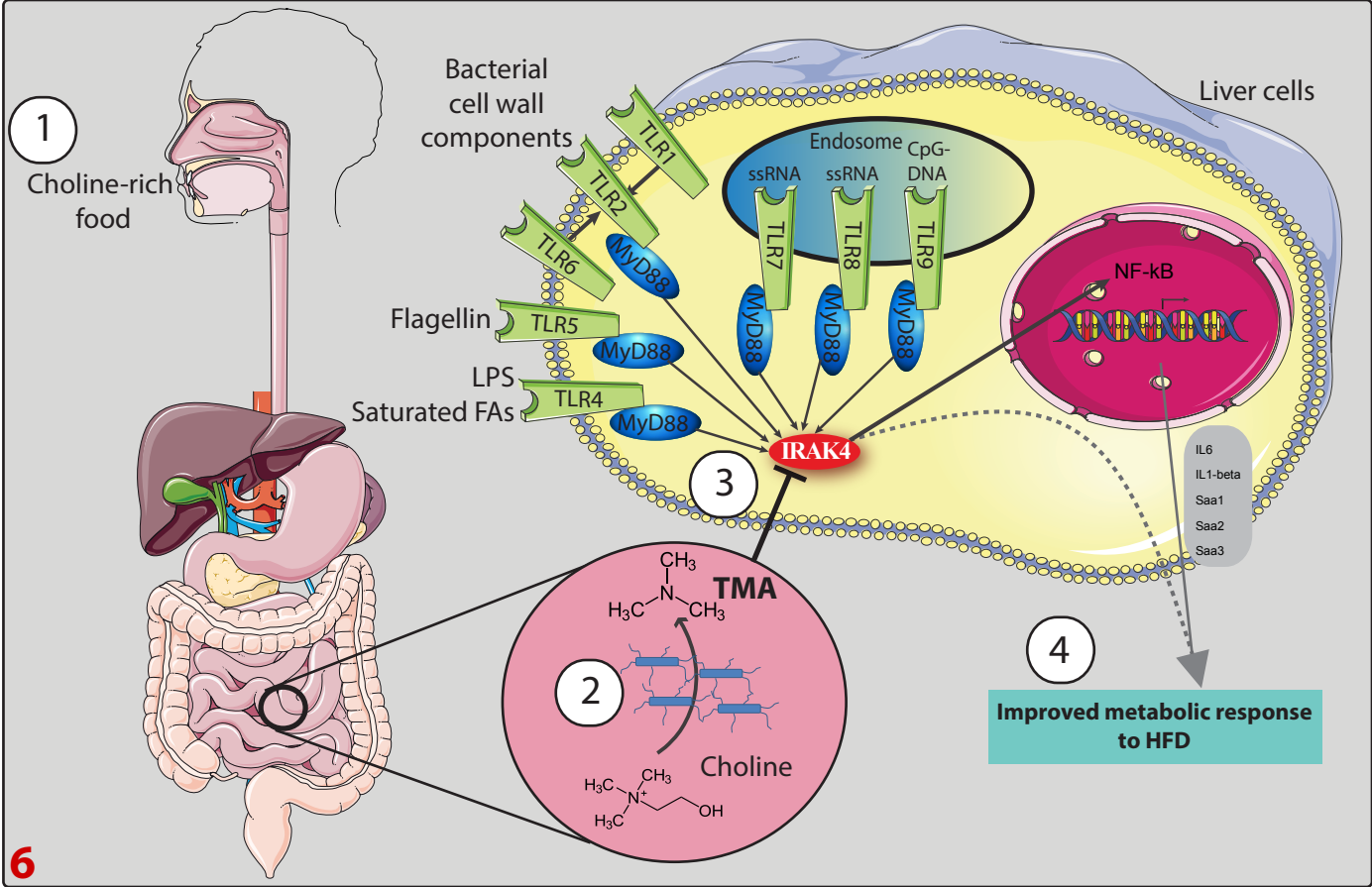
1
Choline-rich food
Bacterial cell wall components
Liver cells
Endosome
ssRNA
ssRNA
CpG-DNA
TLR1
TLR2
TLR6
TLR5
TLR4
TLR7
TLR8
TLR9
MyD88
Flagellin
LPS
Saturated FAs
IRAK4
NF-kB
IL6
IL1-beta
Saa1
Saa2
Saa3
3
TMA
2
Choline
4
Improved metabolic response to HFD